SMALL EXTRACELLULAR VESICLE LOADED 3D BIOPRINTED CARDIAC PATCH FOR TISSUE REPAIR POST MYOCARDIAL INFARCTION

A Dissertation
Presented to
The Academic Faculty

by

Pranshu Rajurkar

In Partial Fulfillment
of the Requirements for the Degree
Master of Science in Biomedical Engineering in the
Wallace H. Coulter Department of Biomedical Engineering

Georgia Institute of Technology and Emory University
MAY 2024

SMALL EXTRACELLULAR VESICLE LOADED 3D BIOPRINTED CARDIAC PATCH FOR TISSUE REPAIR POST MYOCARDIAL INFARCTION

Approved by:

Dr. Michael E. Davis, Advisor
School of Biomedical Engineering
Georgia Institute of Technology

Dr. Vahid Serpooshan
School of Biomedical Engineering
Georgia Institute of Technology

Dr. Hanjoong Jo
School of Biomedical Engineering
Georgia Institute of Technology

Date Approved: April 25, 2024

To my family, my mentors and all the international scholars who dared to fly far away from their homes to pursue their dreams. You inspire me every day.

ACKNOWLEDGEMENTS

First of all, I would like to sincerely thank my thesis advisor, Dr. Michael Davis. He agreed to let me join his lab with only one year left to pursue my master's thesis and allowed me to propose and work on a new idea from scratch. He has been incredibly supportive and encouraging, providing constructive criticism, and helping find a way forward whenever I was stuck on a problem. I am also extremely grateful to Dr. Vahid Serpooshan in whose lab I learnt the basics of 3D bioprinting and Dr. Hanjoong Jo, both of whom graciously agreed to be on my thesis committee.

A huge thank you to all the members of the Davis Lab for creating the most enjoyable environment for pursuing research. Thank you to Felipe, who taught me how to isolate extracellular vesicles, perform assays to characterize them and answered several of my questions on a daily basis. The project would not have been possible without the constant support of Olga and Kenneth who were always available to help in troubleshooting experiments when things did not go according to plan. I gratefully acknowledge the assistance provided by the ICI Core at Emory University, especially Hunter, for training me on the confocal microscope and the Tirouvanziam Lab at Emory University for letting me use their NTA machine.

A special thank you to my dear friend and flat mate Vani Sridhar for her unwavering support, always pushing me to do my best. Finally, I would like to extend my deepest gratitude to my parents for always believing in me, giving me the courage to dream big, and the confidence required to pursue it.

TABLE OF CONTENTS

LIST OF TABLES

LIST OF FIGURES

LIST OF SYMBOLS AND ABBREVIATIONS

MI	Myocardial infarction
CVD	Cardiovascular disease
CM	Cardiomyocyte
SC	Stem cell
EV	Extracellular vesicle
sEV	Small extracellular vesicle
MSC	Mesenchymal stem cell
HSC	Hematopoietic stem cell
iPSC	Induced pluripotent stem cell
MVB	Multivesicular bodies
ILV	Intraluminal vesicles
CPC	Cardiac progenitor cell
3D	Three dimensional
PLGA	Poly-lactic-co-glycolic acid
GelMA	Gelatin methacrylate
NP	Nanoparticle
NTA	Nanoparticle tracking analysis
BCA	Bicinchoninic acid
HUVEC	Human umbilical vein derived endothelial cell
FBS	Fetal bovine serum
BM-MSC	Bone marrow derived MSC
EGM	Endothelial growth medium

EBM	Endothelial basal medium
LAP	Lithium phenyl-2,4,6-trimethylbenzoylphosphinate
UV	Ultraviolet
PBS	Phosphate buffer saline
SEM	Scanning electron microscopy
TEM	Transmission electron microscopy
CAD	Computer aided design

SUMMARY

Myocardial infarction is a leading cause of morbidity worldwide, often leading to heart failure and death caused by severe damage to the cardiac tissue. While stem cells therapies have been explored to regenerate the injured tissue, they suffer from tumorigenicity, immune rejection, low engraftment rates and poor translation overall. Recently, small extracellular vesicles (sEVs), the mediators of paracrine signaling for stem cells, have emerged as cell-free therapies and have been shown to possess cardioprotective and regenerative potential. However, sEV therapies suffer from poor tissue targeting and fast clearance from the circulation when injected intravenously or locally. To overcome these shortcomings, the goal of this study was to fabricate a sEV loaded 3D bioprinted cardiac patch. We hypothesized that once implanted on the injured heart tissue, the patch will be able to control the release of the encapsulated sEVs and retain them on-site for better regenerative outcomes. We isolated sEVs from cardiac progenitor cells (CPC) and successfully fabricated a 3D bioprinted cardiac patch which sustained the release of the encapsulated sEVs for over two weeks. We showed that the CPC sEVs had a strong angiogenic, pro-proliferative and pro-migratory effect on endothelial cells and this functionality was retained by the sEV loaded patch in vitro. Taken together, this study demonstrates the potential of 3D bioprinted sEVs for cardiac tissue regeneration and sets a strong foundation for in vivo studies in the future.

CHAPTER 1. INTRODUCTION

Myocardial infarction (MI) is among the most common cardiovascular diseases (CVD) resulting in damage to the heart muscle[1]. It is caused by a reduction or complete restriction of blood flow to an area of the heart leading to localized necrosis of the cardiac tissue[2]. Since the adult cardiomyocytes (CM) are largely non-proliferative[3], the damaged myocardium is usually replaced by fibrotic tissue, causing arrhythmia, ventricular remodeling and eventually heart failure[4,5]. With an estimate of 0.8 million events occurring yearly in the United States alone, heart failure is a leading cause of morbidity and mortality globally[6] necessitating the development of novel therapies.

1.1 Stem Cells for Cardiac Tissue Regeneration

Via lineage tracing of the regenerated heart tissue, it has been observed that the newly formed cardiomyocytes originate from stem cells (SC)[7]. Consequently, stem cell therapy has emerged as a potential solution for cardiac tissue repair and it serves two benefits. Firstly, transplanted SCs can differentiate into functional CMs[8] and secondly, through the secretion of paracrine factors, SCs can promote cell proliferation and angiogenesis while inhibiting apoptosis and fibrosis at the site of injury[9]. However, intrinsic challenges such as the potential for tumorigenicity[10], low retention and engraftment rates[11], immunological intolerance[12], storage and transportation of cells, and stringent regulatory requirements[13] lead to poor clinical outcomes and limit the translation of SC therapies. More recently, it has been shown that the regenerative potential of these SCs can be largely attributed to the extracellular vesicles secreted by the them[14]. These extracellular vesicles (EV), particularly small extracellular vesicles (sEVs) or exosomes

isolated from several types of cells such as mesenchymal stem cells (MSC)[15], hematopoietic stem cells (HSC)[16], induced pluripotent stem cells (iPSC)[17] and even cardiac progenitor cells (CPC)[18] have demonstrated cardioprotective effects and offer a promising cell free alternative to SC therapies.

1.2 Small Extracellular Vesicles for Cardiac Tissue Regeneration

sEVs are membranous vesicles with diameters ranging from 30 to 150 nm derived from the endosomes formed by the plasma membrane of cells[19]. As the endosomes mature, their inward budding leads to the formation of multivesicular bodies (MVB) containing several intraluminal vesicles (ILV)[20]. Throughout this process, a significant portion of cytoplasmic inclusions become incorporated into the ILVs making them natural carriers of DNA, mRNA, microRNA, and proteins[21]. These ILVs are released as sEVs when the MVBs fuse with the plasma membrane. Besides being carriers of signaling molecules, sEVs do not induce immune responses in the host, thus avoiding the problem of immune rejection faced by SC therapies[22]. Composition of the sEVs varies depending on the cell of origin and its pretreatment or environment. Currently, sEVs derived from mesenchymal stem cells are a major area of focus due to their ability to promote differentiation, angiogenesis, proliferation, and cardiac repair, among other functions[23]. sEVs obtained from CPCs are also gaining increased attention as they have been shown to reduce cardiomyocyte apoptosis, promote proliferation of endothelial cells and improve overall cardiac function after myocardial infarction[24].

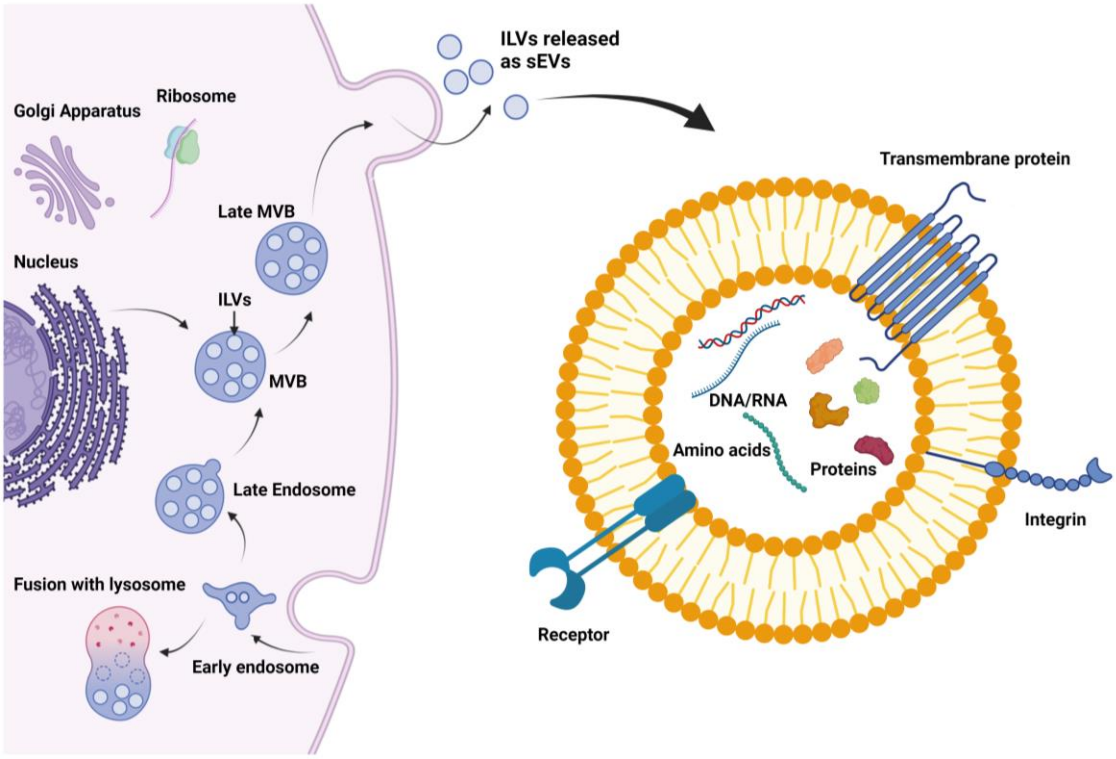

Figure 1- Overview of the biogenesis and contents of small extracellular vesicles. Endosome formed by inward budding matures into a multivesicular body and merges with the cell membrane releasing its intraluminal vesicles as sEVs. sEVs serve as natural carriers of several signaling molecules.

However, there are challenges in the successful clinical translation of sEV-based regenerative therapies. The primary concern is to ensure the delivery of the sEVs to the designated tissue or organ. Due to their small size, sEVs are usually removed from circulation and accumulate mainly in the spleen and the liver in less than a day after systemic administration[25]. To overcome this, multiple doses at short intervals are required to prolong the therapeutic effects. However, repeated administration my lead to abnormally high levels of sEVs in tissues or plasma, leading to off-target effects in peripheral organs. Even when administered locally at the cardiac site, due to high hemodynamics of the region, the EVs are cleared from the heart tissue within 3 hours[26]. Enabling the retention

and controlled release of sEVs at the site of tissue damage remains a significant challenge. During the past decade, encapsulation of sEVs in polymeric scaffolds and particularly hydrogels has emerged as an increasingly popular solution for their sustained loco-regional delivery.

1.3 Hydrogels and 3D bioprinting for sEV delivery

Hydrogels have been successfully explored for applications in the in-vivo delivery of cells, drugs, and nanomaterials. With their complex three dimensional structure and remarkable ability to retain water and bodily fluids, hydrogels closely mimic the native extracellular matrix[27]. Furthermore, due to their bioactivity, high biocompatibility and ease of functionalization, hydrogels have been extensively used in tissue regenerative applications[28]. Notably, hydrogels can also serve as effective scaffolds for the protection, encapsulation, retention, and controlled release of sEVs[29]. Besides allowing for their sustained release, the hydrogel scaffolds also work synergistically with the sEVs enabling the recruitment of endogenous cells and providing a conducive environment for their proliferation thus collectively augmenting tissue regeneration. sEV loaded hydrogels, particularly injectable hydrogels are being actively explored as cell-free alternatives for repairing and regenerating damaged tissue post myocardial infarction and have been shown to significantly improve cardiac function[30,31,32]. Although injectable and casted hydrogels have attracted considerable attention in the regenerative medicine field, they have certain limitations which hamper their translation in-vivo. These include- a. absence of a specific structure, b. very low porosity to allow vascularization, c. potential toxicity of unreacted crosslinkers in in-situ gelling formulations, d. clotting within syringe leading to loss of

sEVs, and e. poor control over the sEV distribution within the injected hydrogel patch[33,34]. 3D bioprinting holds the potential to overcome these limitations.

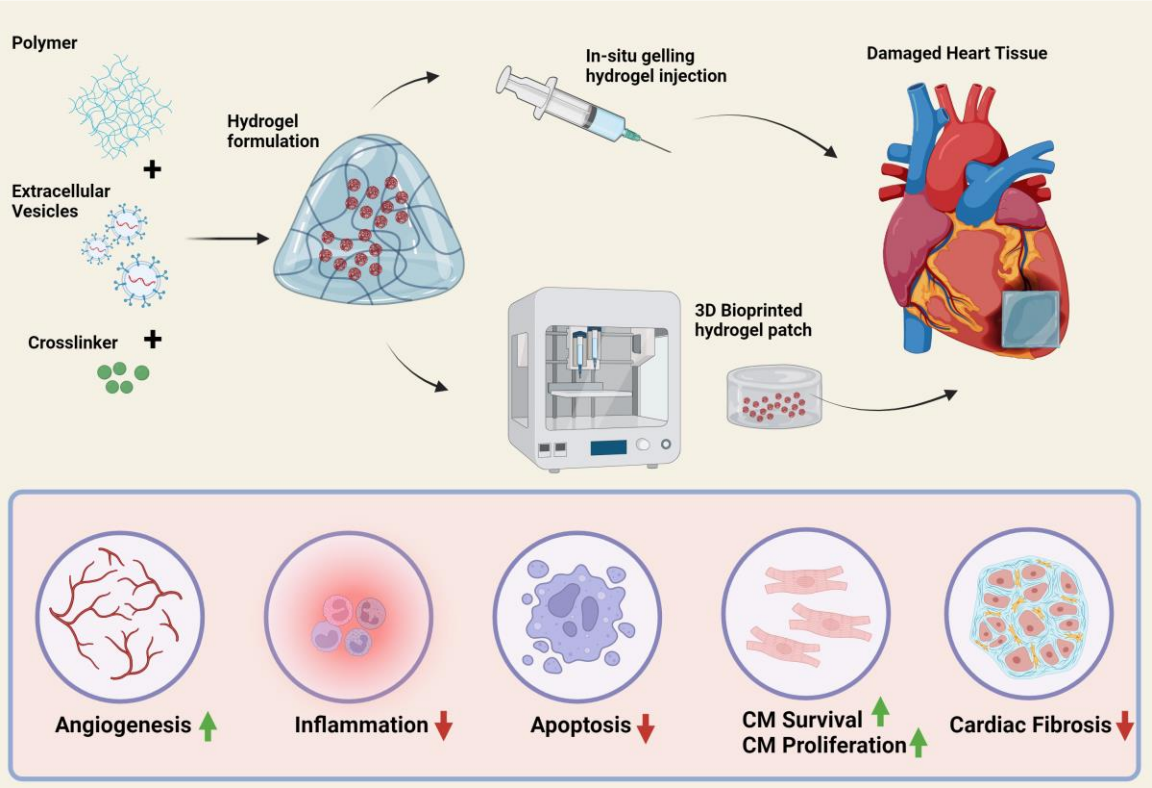

Figure 2- sEV loaded hydrogel formulations for cardiac tissue regeneration. sEVs delivered to the damage cardiac tissue via injectable or 3D bioprinted hydrogels have enhanced on-site retention leading to effective cardio-protection and tissue regeneration.

3D Bioprinting is a form of additive manufacturing and a rapidly developing field in regenerative medicine. It uses a mixture of biomaterials, cells, and bioactive molecules to print elaborate 3D structures which either mimic native tissues for use as in-vitro models or as a delivery vehicle for regenerative therapeutics[35,36]. While 3D bioprinting has been widely explored for the delivery of cells, growth factors and nanoparticles, bioprinting with EVs is a very new concept first published only four years ago[37]. By effectively controlling the fabrication parameters, 3D bioprinted patches provide the following advantages over

injectable hydrogels for sEV delivery- a. personalized design of the bioprinted construct modeled using digitally acquired shape of the defect in the patient, b. precise control over the fiber diameter, pore size and structure of the construct allowing controlled delivery and optimal vascularization, c. ability to print multiphasic constructs with control over the distribution of biomaterials and EVs enabling regeneration of complex tissue structures. Due to these advantages, since 2019, 3D bioprinted sEVs loaded constructs have been explored for applications in bone regeneration[38,39,40,41], cartilage regeneration[42,43,44,45], neural tissue regeneration[46,47], diabetic wound healing[48] and cardiac tissue regeneration[49,50]. However, to adequately incorporate and release sEVs from bioprinted substrates the choice of bioprinting modality, sEV loading quantity, bioink selection, crosslinker concentration and construct structure must be optimized[51,52,53,54].

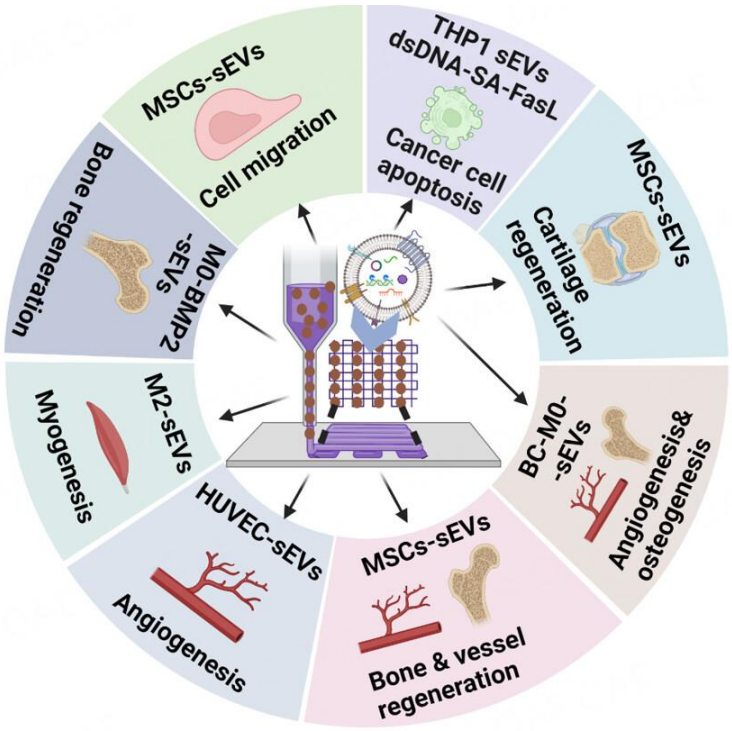

Figure 3- Applications of sEV loaded 3D bioprinted patches. Adapted from Han et. al[34]. under Creative Commons License 4.0.

In the field of cardiac regeneration, several studies have also explored stem cell loaded bioinks for 3D printing cardiac patches[55,56], however, a critical limitation of this approach is the low viability and survival of cells within the patch. For the only two published works on cardiac tissue regeneration using 3D bioprinted sEVs, THP-1 macrophage derived sEVs were incorporated into stem cell loaded cardiac patches either to improve the viability of the encapsulated cells or to improve the attachment of the patch to the cardiac tissue. Although highly promising, there have not been any studies on developing completely cell-free sEV loaded cardiac patches yet. Recently, 3D bioprinted MSC-sEVs have been shown to promote endothelial cell migration in-vitro, however its application in cardiac tissue engineering was not addressed[52]. Besides, CPC derived sEVs which are highly cardioprotective have never been used for bioprinting.

To address this niche, the goal of our study was to develop a modular cell-free 3D bioprinted platform for delivering functional sEVs to the cardiac tissue for promoting tissue repair post myocardial infarction. To this end, we fabricated human neonatal CPC derived sEV loaded cardiac patches using a gelatin methacrylate bioink. The patches were able to sustain the release of the encapsulated sEVs for over 14 days and had the ability to promote angiogenesis, migration, and proliferation of endothelial cells in-vitro. The preliminary in-vitro results indicate the therapeutic potential of the GelMA-sEV patch and set the foundation for conducting in-vivo studies in the future.

CHAPTER 2. SPECIFIC AIMS

The objective of this study is to develop a cell-free 3D bioprinted sEV loaded cardiac patch which can sustain the release of sEVs and test the functionality of the patch in vitro. We hypothesize that by encapsulating MSC and CPC derived sEVs in a 3D bioprinted cardiac patch, we can control their release over 14 days while maintaining their angiogenic and pro-migratory properties. To test our hypothesis, we pursued the following specific aims:

2.1 Fabrication of a fluorescent nanoparticle (NP) loaded 3D bioprinted patch to assess nanoparticle distribution and optimize release profile

Since the isolation of sEVs is an expensive and lengthy process, we will use fluorescent poly lactic-co-glycolic acid (PLGA) NPs with 200 nm diameter as their substitutes for preliminary non-functional testing. Patches will be printed using a bioink composed of gelatin methacrylate (GelMA) and PLGA NPs. The uniformity of distribution of NPs in the patch will be analyzed using laser confocal microscopy and the bioink formulation will be optimized to generate the desired NP release profile

2.2 Characterization of sEVs isolated from MSCs and CPC and the subsequent sEV loaded 3D bioprinted patch

sEVs will be isolated from MSCs and CPCs via ultracentrifugation and characterized for their size and count using nanoparticle tracking analysis (NTA), protein concentration using the bicinchoninic assay (BCA), angiogenic ability using the tube formation assay and pro-migratory potential using the scratch wound healing assay. Patches will be printed with a bioink composed of GelMA and sEVs stained with a fluorescent dye. The uniform

distribution of sEVs in the patch will be verified via laser confocal microscopy and the sEV release profile from the patch will be analyzed.

2.3 Assessment of in vitro pro-migratory and pro-proliferative potential of the sEV loaded cardiac patch

The pro-migratory potential of the patch will be studied by preconditioning HUVECs with the sEV loaded patch using a transwell chamber followed by the scratch wound healing assay. To test the pro-proliferative ability of the patch, the rate of growth of human umbilical vein endothelial cells (HUVEC) in the presence of the sEV loaded patch will be analyzed over two days using the MTS assay and compared against controls.

The results of this study will contribute towards the development of a completely cell free cardiac patch for heart tissue repair and set the stage for in-vivo experimentation and possible clinical translation.

CHAPTER 3. MATERIALS AND METHODS

3.1 Neonatal human cardiac progenitor cell isolation and culture

The harvesting of human neonatal CPCs expressing c-kit from the atrial appendage was approved by the Institutional Review Board at Children's Healthcare of Atlanta and Emory University. Pediatric patients with the age of one week or lower undergoing surgery for congenital heart disease were considered for obtaining the right atrial appendage tissue. 1 mg/mL collagenase type II (300 U/mL) (Worthington, NJ, USA) was used to enzymatically degrade the excised tissue at 37ºC, 5% CO2 for 30 minutes and subsequently passed through a 70 µm filter. The filtrate was centrifuged for 5 minutes at 1200 rpm to pellet the cells which were further purified via repeated magnetic sorting using Dynal magnetic beads (Invitrogen, CA, USA) conjugated with anti-c-kit antibody (Santa Cruz, TX, USA). These c-kit positive CPCs were grown in Ham's F-12 culture media (Corning Cellgro, NY, USA) supplemented with 1% Pen-Strep (Corning Cellgro, NY, USA), 1% L-glutamine (MP Biomedicals, OH, USA), 10% fetal bovine serum (FBS) (Hyclone, TX, USA) and basic fibroblast growth factor (bFGF) (Stemcell technologies, Canada). Media was changed every 2-3 days until the isolation of sEVs from the CPCs.

3.2 MSC and HUVEC cell culture

Human bone marrow derived mesenchymal stem cells (BM-MSC) were purchased from Gibco (StemPro™ BM Mesenchymal Stem Cells, Gibco, Waltham, MA) and HUVECs were purchased from Lonza (HUVEC, Pooled, in EGM™-2, Lonza, Basel, Switzerland). MSCs were cultured in Dulbecco's Modified Eagle Medium and Ham's-F-

12 medium (DMEM/F12 50/50 1X, Corning Cellgro, NY, USA) supplemented with 10% FBS, 1% pen-strep and 1% L-glutamine. Media was changed every 2-3 days until the isolation of sEVs from the MSCs. HUVECS were cultured in Endothelial Basal Medium-2 (EGM-2™) supplemented with 0.1% Herparin, 0.1% Gentamycin sulphate, 0.1% rhEGM Epidermal Growth Factor, 0.1% Ascorbic Acid, 0.1% R3-IGF-1 Insulin like Growth Factor, 0.1% Vascular Endothelial growth Factor, 4% rhFGF Fibroblast Growth Factor, 0.04% Hydrocortisone (EGM™-2 Endothelial Cell Growth Medium-2 BulletKit™, Lonza, Basel, Switzerland), 2% FBS, 0.2% L-Glutamine and 0.2% Pen-Strep as per manufacturers protocol. Media was changed every 2-3 days to continue growth.

3.3 Small extracellular vesicle isolation

CPCs (between passages 9-13) and MSCs (between passages 15-20) were grown until 15 T-175 flasks at 90% confluency (~200×10^6 cells) were obtained. On reaching confluency, the culture media was replaced with FBS-depleted basal media and the conditioned media was collected after 24 hours. To isolate sEVs from the conditioned media, differential ultracentrifugation (Optima XPN-100, Beckman Coulter, Indianapolis, IN) was used. Briefly, the conditioned media was depleted of cells by centrifugation at 1000 RPM for 5 minutes (Centrifuge 5810 R, Eppendorf, Hamburg, Germany). Cell debris along with medium and large EVs were depleted at 15,000 RPM and 4^0C for 30 minutes (SW32Ti, Beckman Coulter) and the supernatant was collected. The supernatant was centrifuged at 31,000 RPM and 4^0C for 2 hours (SW32Ti, Beckman Coulter) to concentrate sEVs at the bottom of the centrifuge tube and the bottom 5 mL were collected. This sEV concentrated condition media was pooled and centrifuged again at 31,000 RPM and 4^0C for 2 hours (SW32Ti, Beckman Coulter) to pellet the sEVs. 1 mL from the bottom of the

centrifuge was collected and resuspended in PBS as required and stored at -80^{0}C until further use.

3.4 sEV characterization

The size and concentration profiles of the sEVs obtained from CPCs and MSCs were quantified via Nanoparticle Tracking Analysis NTA (Nanosight NS-300 with NTA 3.4 software, Malvern Panalytical, Malvern, UK). Briefly, the sEV samples were loaded onto a syringe pump and pumped into a microfluidic channel. Three 60 second videos of sEVs flowing through the channel were captured per sample and analyzed using the above-mentioned software to calculate the sEV size and concentration. The protein concentration of the sEVs was calculated using the bicinchoninic acid assay (Pierce™ BCA Protein Assay Kit, Thermo Fisher Scientific, Waltham, MA) or the micro- bicinchoninic acid assay (Micro BCA™ Protein Assay Kit, Thermo Fisher Scientific, Waltham, MA) as per the manufacturer's protocol. An incubation time of 1 hour and 2 hours was used for the BCA and the µ-BCA assay respectively.

3.5 Staining of sEVs

The CPC and MSC derived sEVs were fluorescently stained using the green fluorescent lipophilic dye DiO (Vybrant™ DiO Cell-Labeling Solution, Thermo Fisher Scientific, Waltham, MA) followed by dialysis (Float-A-Lyzer™ G2 Dialysis Device, SpectraPor, Repligen, Waltham, MA) to remove the unbound dye. Briefly, the dialysis device with 1 mL volume and 8-10 kDa molecular weight cut-off was pre conditioned following the manufacturer's instructions. The sEV suspension and the DiO solution in the ratio 10:1 was mixed together at 37^{0}C for 30 mins under constant rotation to allow the

sEVs to be stained. This mixture was transferred into the preconditioned Float-A-Lyzer™ device and dialyzed for 16 hours in 2 liters of PBS under mild agitation to remove the unbound DiO. The volume of the dialyzed product was measured to calculate the dilution factor and it was stored at -80^{0}C until further use.

3.6 Bioink preparation

Gelatin methacrylate (GelMA) was assessed to be a suitable hydrogel for this study based on prior works from our lab and others[57,58]. It is highly biocompatible and supports extrusion 3D bioprinting with high fidelity. GelMA in the form of a lyophilized product was purchased from CELLINK (PhotoGel® 50% DS, CELLINK, Gothenburg, Sweden). GelMA solutions of 15% were created by adding PBS to the lyophilized GelMA and allowed to dissolve under stirring at 70ºC for 1 hours followed by vortexing to homogenize the solution. These stock solutions were frozen at -20ºC until further use. GelMA bioinks for extrusion printing were prepared by mixing the GelMA stock solution (final concentration 7% w/v), Lithium phenyl-2,4,6-trimethylbenzoylphosphinate (LAP Powder, CELLINK, Gothenburg, Sweden) (final concentration 0.2% w/v) as the photo initiator and PBS. In the case of GelMA-NP bioink, the PBS in the above formulation was replaced by a NP suspension in PBS such that the final concentration of the NPs in the GelMA bioink was 10 billion NPs/mL. Fluorescent NPs with 200 nm average diameter were purchased from Sigma-Aldrich (Degradex® Green Fluorescent PLGA nanoparticles, Sigma-Aldrich, Darmstadt, Germany). To formulate GelMA-sEV bioink, the PBS in the initial formulation was replaced with either a stained sEV or non-stained sEV suspension in PBS such that the final concentration of the sEVs in the bioink was 10 billion sEVs/mL. To make the GelMA-NP and GelMA-sEV bioinks homogenous, the mixing cells and bioinks protocol by

CELLINK was followed. For all the bioinks, the final GelMA and LAP concentrations remained constant. The formulated inks were loaded in a sterilized 3 mL UV shielding bioprinting cartridge (CELLINK, Gothenburg, Sweden), stored at -20^{0}C overnight and used on the following day.

3.7 Bioprinting and patch formation

All the bioinks- GelMA, GelMA-NP and GelMA-sEV underwent similar printing protocols. A sterile 27 gauge conical bioprinting nozzle (CELLINK, Gothenburg, Sweden) was attached to the previously prepared bioink loaded cartridge and the cartridge was inserted into the temperature controlled printhead of the BIO X extrusion bioprinter (CELLINK, Gothenburg, Sweden) set at 27^{0}C. The bioink was allowed to equilibrate for 1 hour in the printhead before printing. The printhead was calibrated and purged for 1-3 seconds at 20 kPa pressure to ensure free flow of the bioink. The patches were disks with 10 mm diameter and 1 mm height designed on SolidWorks. All patches were printed in 6 well plates at 30-40 kPa pressures with the printing speed of 20 mm/s. Patches were 10 mm in diameter and 1 mm thick, which printed in 5 layers, with an infill pattern of 90º grids and an infill density of 25%. Test grids were printed on an imaging dish (µ-Dish 35 mm, ibidi GmbH, Germany) with the GelMA-NP bioink as boxes with dimensions 10 mm × 10 mm, an infill pattern of 90^0 grids and a spacing of 1mm. The CAD (computer-aided design) models of the patches and the test grids were designed on SOLIDWORKS (Dassault systems, France) and imported to and sliced using the bioprinter. After printing, the patches and test grids were crosslinked using a 405 nm UV light source (JAYO, China) for either 45 or 90 seconds. The patches were then hydrated in 2 mL PBS for 1 minute,

removed for imaging or transferred to a 48 well plate or a transwell chamber for further experiments.

3.8 Patch imaging

Brightfield images of the printed patches and test grids were taken at 4x magnification with an Olympus 1X71 Inverted Microscope. To assess the distribution of fluorescent nanoparticles (Excitation/Emission- 460/500 nm) and stained sEVs (Excitation/Emission- 484/501 nm), the patches were transferred to an imaging dish (µ-Dish 35 mm, ibidi GmbH, Germany) and imaged at 4x and 10x magnification using a laser confocal microscope (CSU-W1 SoRa Spinning Disk Microscope, Nikon, Japan) to obtain full thickness Z stacks. All images were processed on the ImageJ software (Fiji, National Institutes of Health, Bethesda, MD).

3.9 Patch swelling and degradation

GelMA patches were printed as described above and immersed in PBS for 24 hours to allow swelling. The swollen patches were weighed (wet weight) and then transferred to a desiccator for 2 days. The weight of the dry patch was then measured (dry weight) and the swelling ratio was calculated as wet weight/dry weight. Patch degradation was assessed by measuring weight change of the patch over time. Briefly, the patches were first swelled for 24 hours in PBS. To measure patch degradation via weight change, the patches were weighed on days 1, 3, 7, 10 and 14 days after printing. Degradation via hydrolysis was determined as the change in weight compared to original weight at day 1.

3.10 Printability analysis

The printability analysis employed here tests the ability of the bioink to form square holes in the test grids as described previously[59]. The circularity of a hole is calculated using its area and perimeter and a circle has a circularity value of 1. The circularity of a square shape is π/4. To this end, the printability of a square hole is given by the Equation 1

$$Pr = \frac{\pi}{4} * \frac{1}{C} = \frac{L^2}{16A} \quad (1)$$

Where A is the area and L is the perimeter of the shape. The printability of 1 indicated a perfect square which shows optimal printing and gelation conditions for the bioink. Brightfield images of the test grids were taken and a total of 20 holes (4 holes each from 5 test grids) were evaluated for printability using ImageJ and the Equation 1.

3.11 NP and sEV release from the patch

The printed GelMA-NP or GelMA-sEV patches were transferred to a 48 well plate. 300 µL of PBS was added in each well and the plate was incubated at 37^0C for 14 days. At 1 hour, 3 hours, 6 hours, day 1, day 2, day 4, day 7 and day 10, all the PBS from each well was collected and replaced with fresh PBS. The collected release media was stored at -20^0C until further analysis. On day 14, the collected release medium was replaced with 30 U/mL solution of collagenase I in PBS. The patch was incubated at 37^0C for 4-6 hours to allow the complete degradation of GelMA and the complete release of NPs or stained sEVs in the media. To measure the release of NPs or sEVs from the patch, 200 µL of the release medium collected at each time point was transferred to a 96 well plate and the fluorescent intensity was measured using a plate reader (BioTek Synergy 2, Agilent Technologies, CA, USA). 3-4 technical replicates were used at each collection time point.

3.12 Tube formation assay

HUVECs were cultured as previously described until they were 90% confluent. Before the experiment, the cells were quiesced for 16 hours by replacing the growth media with serum free basal media. A µ-slide Angiogenesis slide (ibidi GmbH, Germany) was prepared by carefully adding 10 µL of Geltrex™ (Thermo Fischer Scientific, Waltham, MA) in each well according to manufacturer's instructions. The plate was then centrifuged at 1000 RPM for 2 mins before curing at 37^0C for 1 hour to remove any bubbles. The 10,000 quiesced HUVECs were then added to each coated well. For the treated group, sEVs were added to wells at the concentration of 2000 sEVs per HUVEC and cultured for 12 hours in basal medium. HUVECs were then stained with 30 µL of Calcein-AM (Thermo Fischer Scientific, Waltham, MA) at the concentration of 0.003 mM for 30 mins and imaged at 4x magnification using a fluorescent microscope (Olympus IX71) such that a complete well was covered in one image. Different tube parameters were measured using the ImageJ software and an angiogenesis analyzer plugin designed specifically to assess the vascular structure of endothelial cells was used to quantify the images. Data corresponding to the total number of branches, total branching length and total tube length was obtained using the plugin. Untreated quiesced HUVECs served as negative controls, while untreated EGM-cultured HUVECs were used as positive controls. At least 3 technical replicates were analyzed for each group.

3.13 Scratch wound healing assay

HUVECs were cultured in EGM as previously described until they were 90% confluent. Subsequently, they were plated into 24 well plates at 100,000 cells per well in

EGM and grown for 48 hours in order to form a confluent monolayer. When confluent, a 200 µL tip attached to a pipette was carefully used to scratch the monolayer diametrically across the well. The pipette tip was held perpendicular, touching the well plate, and moved slowly to create the scratch wound. The monolayer was then washed twice with PBS very gently to remove the detached HUVECs while not disturbing the monolayer and phase contrast images of the scratched wells were taken at 4x magnification using an inverted microscope (Olympus IX71) as pre-treatment images. For the treatment groups, 5 µg of sEVs (by protein concentration measured using BCA) was added to the wells and the cells were cultured in FBS-free EBM. The negative controls did not receive sEV treatment and were cultured in EBM whereas the positive controls did not receive sEV treatment and were cultured in EGM. After 16 hours of incubation, the scratch wounds were imaged again making sure that the same area of the scratch was imaged again. The pre and post incubation images were analyzed using the ImageJ software. A wound healing size tool plugin, specifically designed to assess wound closure was used to quantify the images. Data corresponding to the average scratch width and the total scratch area was obtained using the plugin. At least 3 technical replicates were analyzed for each group. To test the efficacy of the GelMA-sEV patch in promoting HUVEC migration, the HUVECs were pretreated with the patch before generating the scratch. Briefly, the HUVECs were plated at the bottom of 24 well plates with transwell inserts (Transwell® with 8.0 µm Pore Polycarbonate Membrane Insert, Corning, USA) at 100,000 cells per well as previously described. For the treatment group, GelMA-sEV patch with an sEV loading of 10 billion EVs/mL was added to the transwell insert and the cells were grown in EGM for 48 hours to form a confluent monolayer. For the negative controls, GelMA patch (without sEVs) was added

to the transwell insert. Scratches were made in the confluent layer and imaged as previously discussed. The negative controls and the treatment group were then cultured in EBM and the positive control was cultured in EGM for 16 hours. The scratches were then imaged and analyzed as described previously.

3.14 MTS assay for HUVEC proliferation

HUVECs were cultured as previously described until they were 90% confluent. Before the experiment, the cells were quiesced for 16 hours by replacing the growth media with serum free basal media. To optimize cell seeding density and (CellTiter 96® AQ_{ueous} One Solution Cell Proliferation Assay MTS, Promega, USA) incubation times for the MTS assay for future experiments, cells were plated into a 96 well plate at the concentrations of 3.2×10^5, 1.6×10^5, 8×10^4, 4×10^4, 2×10^4, 1×10^4, and 0 cells per plate in 100 µL media with three replicates for each concentration. 20 µL of the MTS reagent (5:1 ratio of media to reagent) was added to the wells and the plate was incubated at 37ºC. At 1, 2 and 3 hours after starting incubation, absorbance of the wells was measured at 490 nm using a plate reader (BioTek Synergy 2, Agilent Technologies, CA, USA) to obtain the absorbance curves. The stained cells were imaged using a fluorescent microscope

To test the efficacy of GelMA-sEV patches in promoting HUVEC proliferation, six experimental groups were designed as shown in the table below (**Table 1**). Briefly, 20000 cells were seeded either in the well or on the construct according to the table. 200 µL final volume of either EBM or EGM was added to each well and the cells were allowed to attach and grow overnight. After 16 hours (Day 1), 40 µL of MTS reagent was added to each well and incubated for 1 hour at 37^0C. After incubation, 100 µL of media was taken from each

well and transferred to a 96 well plate and the color change in the media was measured by quantifying absorbance at 490 nm using the plate reader. GelMA or GelMA-sEV patches from group 4, 5 and 6 were washed with PBS twice and stained with 200 µL of 0.003 mM Calcein AM. The stained cells were imaged using a fluorescent microscope (Olympus IX71). Another experimental set with the same six groups was created and analyzed in the same way to quantify cell proliferation after 40 hours (Day 2). At least 3 technical replicates were analyzed for each group for each time point.

Table 1- Controls and treatment groups for HUVEC proliferation testing

Group- 1: Media Control	EBM	No Patch	No Cells
Group- 2: Patch Control	EBM	GelMA Patch	No Cells
Group- 3: Cell Control	EBM	No Patch	2×10^4 quiesced HUVECS
Group- 4: -ve Control	EBM	GelMA Patch	2×10^4 quiesced HUVECS
Group- 5: Treated group	EBM	GelMA-sEV Patch	2×10^4 quiesced HUVECS
Group-6: +ve Control	EGM	GelMA Patch	2×10^4 quiesced HUVECS

3.15 Statistical Analysis

Numerical data are the mean ± SEM. All data was analyzed using either one-way ANOVAs with Tukey's multiple comparison post-test or unpaired t tests. Sample size (n) was 3-5 for all samples.

CHAPTER 4. RESULTS AND DISCUSSIONS

4.1 Bioprinting and patch characterization

To fabricate a sEV loaded patch that has a high degree of printability, suitable mechanical properties for cardiac regeneration and allows for controlled release of the encapsulated payload, we selected GelMA as our bioink. GelMA is formulated from the natural polymer collagen by functionalizing it with the methacrylate group to allow for its free radical polymerization. Owing to its superior biocompatibility, GelMA has been used as a resorbable and bioactive material for regenerative applications in various tissues such as the liver, muscle, bone and heart[60,61,62,63]. Several other studies have also explored GelMA for encapsulating sEVs successfully as casted[64], sprayable[65] or 3D bioprinted formulations. Using GelMA with LAP as the photoinitiator has been shown to be highly biocompatible upto LAP concentration of 1% w/v[66]. Further, LAP is sensitive to near UV light at 405 nm which is safer than the 365 nm UV light which is required for crosslinking when Irgacure is used as the photoinitiator. Also, unlike stem cells, there are no known negative effects such as loss of functionality, on exposing sEVs to UV radiation at 405 nm. In this study, we used 7% w/v GelMA with 0.2% w/v LAP for the bioink formulation and the patches were fabricated using an extrusion bioprinter. GelMA concentration of 7% w/v was used following the work of Born et. al.[52]. Further analysis is required to measure the stiffness of the constructs printed with this formulation to assess its suitability for cardiac applications, however that was outside the scope of this study. A schematic of the bioink formulation and bioprinting strategy is shown in **Figure 4.**

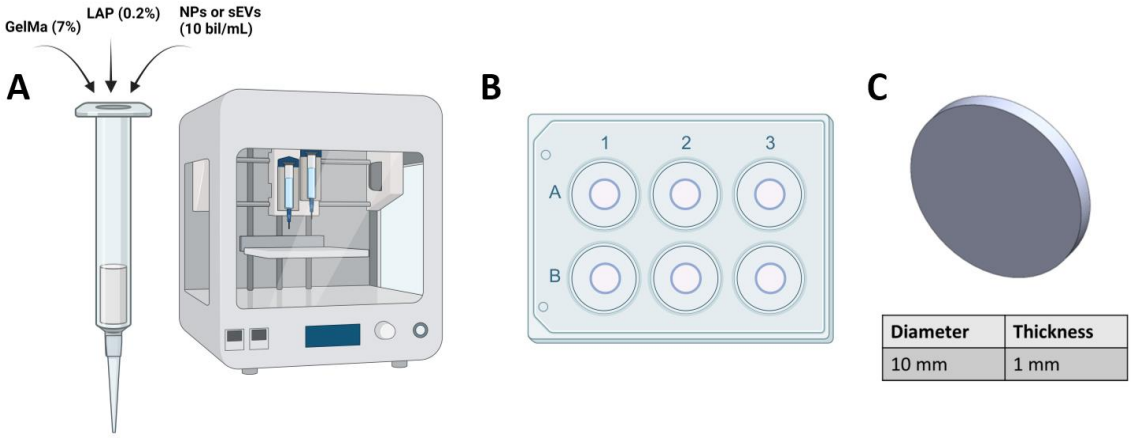

Figure 4- Printing methodology overview. (A) GelMA, LAP and the NPs or sEVs are mixed together in optimized ratios to form the bioink which is loaded into a cartridge with a 27 gauge tip for bioprinting (B) One printing cycle fabricates 6 patches in a 6 well plate (C) CAD model of the cardiac patch

To test the printability of the bioink and ensure that the sEVs are uniformly distributed within the print, fluorescent PLGA NPs were used as sEV substitutes for fabricating a test grid. With a spherical shape and an average diameter of 200 nm, these NPs have a size similar to that of sEVs (100-150 nm). Therefore, we hypothesize that the distribution and the release of NPs from the GelMA-NP patch should closely match the release of sEVs from a GelMA-sEV patch. The printed grids were crosslinked for 45 seconds and imaged using brightfield and laser confocal microscopes showing defined and clean extrusion patters (**Figure 5A**). The green staining in **Figure 5B** depicts the PLGA NPs, indicating that the NPs were homogenously distributed throughout the printed construct, rather than in clumped locations such as filament junctions. Printability of the bioink was measured by assessing the square holes in the grid as described previously. A mean printability of 0.91 depicted high fidelity of the bioprinting process (**Figure 5C**).

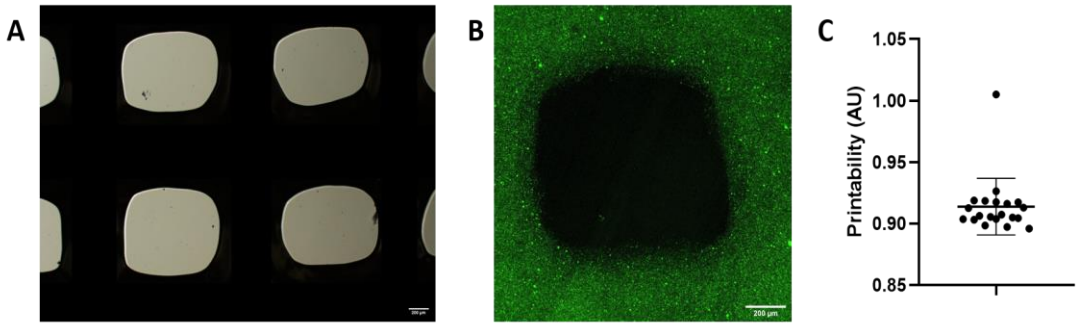

Figure 5- Printability analysis of GelMA-NP bioink. (A) Brightfield image of GelMA-NP test grid. (B) Distribution of NPs in the test grid imaged by laser confocal microscope. (C) Printability of the GelMA-NP bioink (n=20). Scale bar represents 200 µm.

Moving ahead, we fabricated cardiac patches using the GelMA-NP bioink with 10 mm diameter and 1 mm thickness. **Figure 6A** depicts the 3D printed patches having a diameter of 10mm. The internal structure of the patches consisted of perpendicular filament arrangements created across several print layers, showcasing high printing precision and structural integrity. To measure the patch thickness, we used the confocal microscope to obtain a three dimensional projection of the patch prepared from several z stacks (**Figure 6B**). The patch projection had a diameter of 10 mm and a thickness of 1 mm denoting that the patches retained the structure and shape of the CAD model owing to the high printability of the bioink. To ensure that the patches were sufficiently hydrated, we measured their swelling ratio and found it to be between 8.5 and 10 showing that the patches are able to absorb and store water well (**Figure 6C**). Besides serving as a depot for the controlled release of sEVs, the GelMA patches can also serve as scaffolds for tissue regeneration. Thus, the patches should be able to hold their structure during the repair process and their degradation time should be studied. We evaluated the degradation profile of the patches over a period of 2 weeks in PBS by examining the change in their wet weight.

Throughout this time, the patches remained solid and did not degrade significantly (**Figure 6D**). However, it is important to note that the degradation observed here is only due to hydrolysis and does not accurately depict physiological conditions. Further studies are required to precisely estimate the patch degradation in-vivo such as addition of physiologically relevant proteases to the release medium along with exposure to shear stresses and cyclic strains which would be experienced by a patch implanted on the heart.

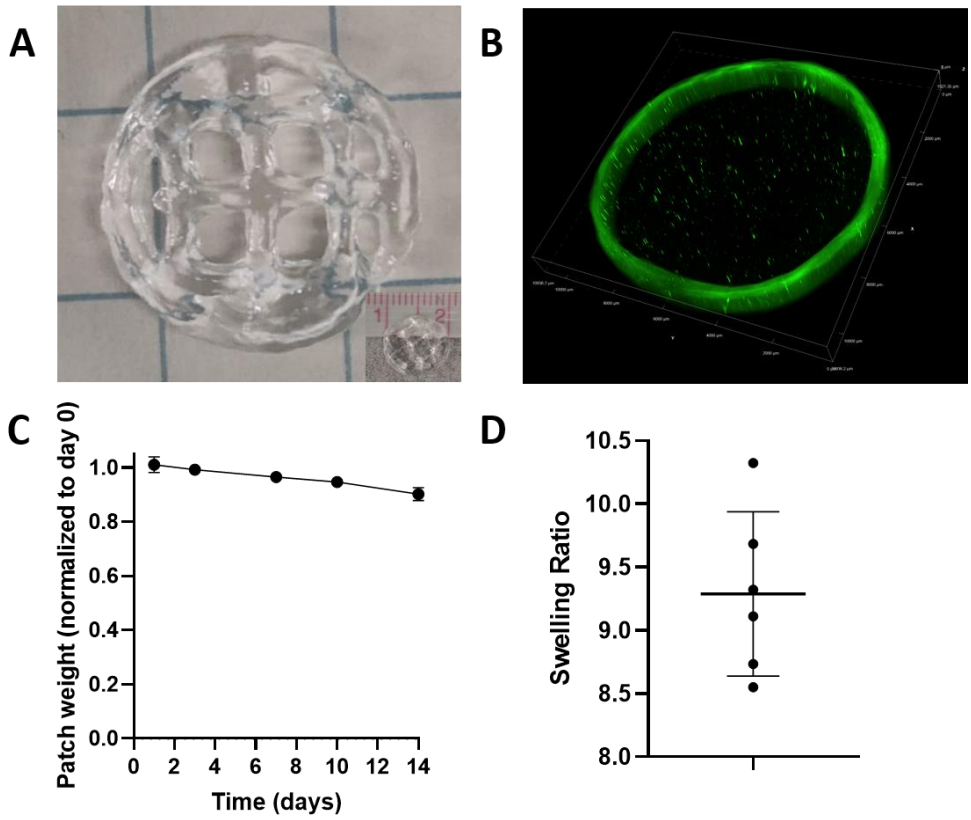

Figure 6- Fidelity and material analysis of the printed patch. (A) Printed GelMA-NP patch with 10 mm diameter and 1 mm height. The infill pattern can be seen in the image (B) 3D projection of the patch via confocal microscope (C) Degradation of the patch in PBS (n=4) (D) Swelling ratio of the patch (n=6).

4.2 Controlled release of NPs from GelMA-NP patch

The main objective of the cardiac patch is to be able to sustain the release of the encapsulated sEVs for upto 14 days when implanted immediately after MI. The rationale behind this time period is as follows. De-novo microvessel formation or angiogenesis has the potential to save ischemic myocardium at the early stages post MI while also preventing a transition into heart failure in the future[67,68]. Post MI, the cardiac tissue undergoes extensive remodeling in 3 stages within 1-2 weeks of injury. (**Figure 7**) Firstly, the ischemic attack leads to localized necrosis of cardiac cells during the first 12 hours. The second inflammatory stage is marked by the invasion of neutrophils and macrophages to clear the dead cells followed by the proliferation phase where fibroblasts and endothelial cells form a granulation tissue in the following two weeks. The vascularization of the granulation tissue along with an increased metabolic demand owing to the mechanical overload on the heart leads to reduced blood supply to the healthy tissue surrounding the infarct and ultimately a decrease in cardiac function. Thus, increased perfusion via neovascularization is required to prevent the death of viable cardiac tissue and prevent further expansion of the infarct during the two weeks after MI. By allowing the release of encapsulated sEVs over 14 days, the cardiac patch can target the remodeling phase post MI, promote angiogenesis, and improve regenerative outcomes. Therefore, in this study, we want to test the ability of sEVs to improve the angiogenesis, migration and proliferation of endothelial cells at the infarct site while improving sEV retention by encapsulating them in a 3D bioprinted cardiac patch.

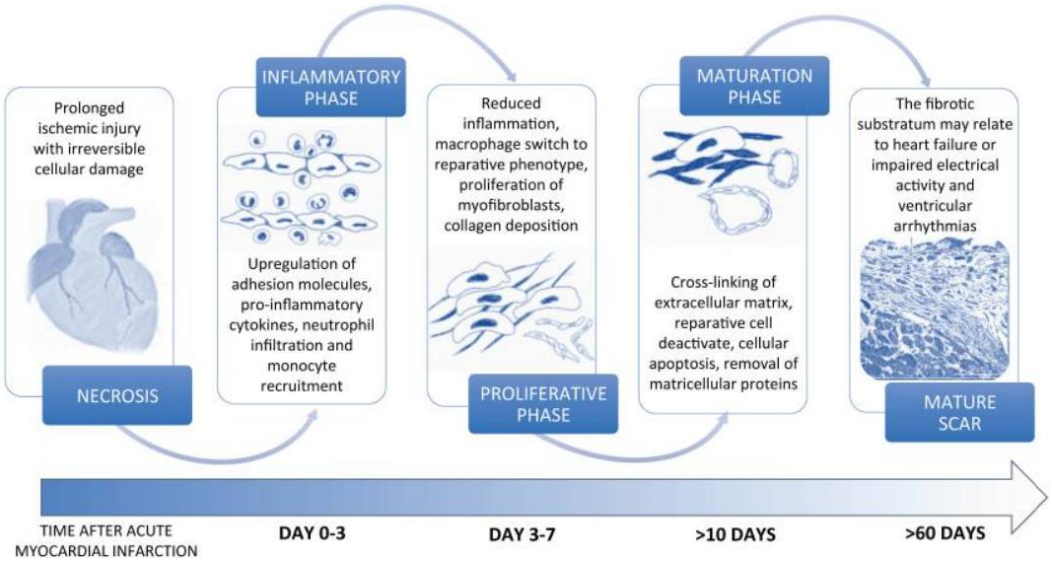

Figure 7- Different phases of healing process after MI. Adapted with permission[69]. Copyright © 2021- MDPI.

The 3D bioprinted GelMA-NP patches were crosslinked for either 45 or 90 seconds with 405 nm UV light and the release of NPs from the patches was studied in either PBS or a 0.2 U/mL collagenase solution. It was observed that following an initial burst release in PBS, the patch was able to sustain the release of NPs over a period of 14 days (**Figure 8**). The release of NPs was marginally faster in the 45 seconds crosslinked GelMA-NP patch as expected; however, the difference was not significant. We hypothesize that most of the GelMA is crosslinked within 45 seconds and thus additional exposure does not contribute to a significant difference in the release characteristics. We used the crosslinking time of 45 seconds for all future experiments. Approximately 30% of the NPs were released in 6 hours and 80% released in two weeks. There are two important mechanisms for the release of NPs from the cardiac patch- diffusion or degradation. The initial burst release is hypothesized to be largely governed by diffusion due to the swelling of the construct, increase in the pore size of the gel scaffold and the creation of a concentration gradient

allowing the NPs to move out of the construct rapidly. During the next 14 days, the slow hydrolytic breakdown of GelMA by PBS leads to the controlled release of NPs from the patch. Additional studies are required to assess the pore size of the GelMA scaffold before and after swelling in PBS, during its degradation over 14 days and its comparison with the size of the encapsulated NPs. This can be done using scanning electron microscopy (SEM) and would shed more light on the release mechanism of the encapsulated NPs. As expected, the GelMA-NP patch degraded completely, releasing all the encapsulated NPs within a day when incubated in the collagenase solution. This is because collagenase is capable of cleaving the polymeric backbone of GelMA leading to its rapid degradation. Again, it is important to note that 0.2 U/mL is a high concentration of collagenase I and is not physiologically relevant. Further studies are required to assess the most accurate release profile of NPs from the scaffold.

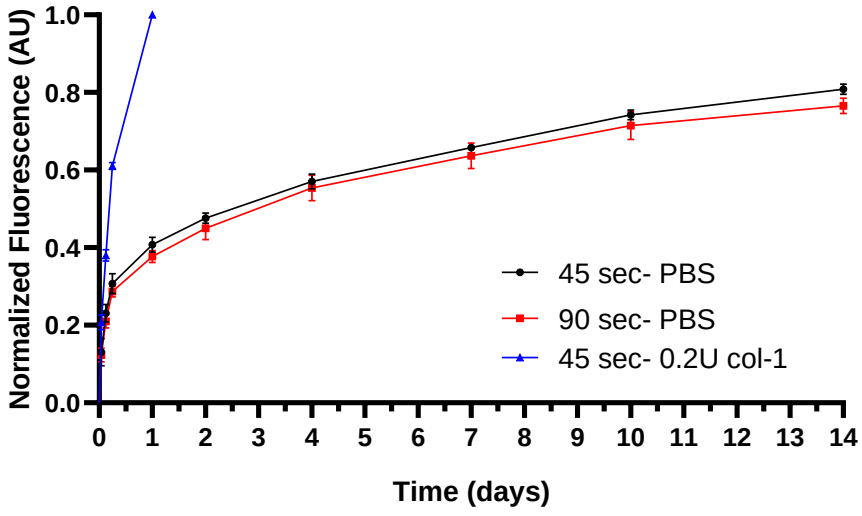

Figure 8- Controlled release of PLGA NPs from GelMA-NP patches. Patches degrade completely within 24 hours in collagenase releasing all NPs however, the NP release is sustained over 14 days in PBS (n=3 for all groups).

4.3 Isolation and characterization of sEVs

Both, CPCs and MSCs (approximately 200 million cells each), were cultured until 90% confluent and their conditioned media was collected. sEVs were isolated from the conditioned media via differential ultracentrifugation. The ultracentrifugation protocol (**Figure 9A**) was optimized to remove cell debris along with medium and large EVs and collect pure and paucidispersed sEVs. The size and concentration of the collected sEVs was analyzed using Nanoparticle Tracking Analysis. The CPC derived sEVs were observed to have a narrow size distribution with a mean diameter of 105.1 ± 5.4 nm, which lies within the expected range (**Figure 9B**). The sEV yield was high with the concentration of $1.05 \times 10^{11} \pm 1.42 \times 10^{10}$ particles/mL. However, the sEVs obtained from the MSCs were observed to be polydisperse. They had a mean diameter of 125.3 ± 1.3 nm with some EVs having a size greater than 200 nm (**Figure 9C**). The yield of the MSC sEVs was $2.13 \times 10^{9} \pm 5.45 \times 10^{8}$ which was 50 times lower than the CPC sEV concentration. The MSCs used for isolating the sEVs were at a high passage number which is associated with mutation of genes responsible for cell cycle regulation, apoptosis, and protein ubiquitination. It has been reported that an increase in the passage number of MSCs leads to decreased sEV production per cell and reduced functionality of the sEVs[70]. We hypothesize that the high passage number is responsible for this lower observed yield. The total protein content of the CPC and MSC sEVs quantified using the BCA and the µ-BCA assay was observed to be 224.27 µg/mL and 10.51 µg/mL respectively. Owing to their higher yield and protein content, only CPC sEVs were used for all further experiments.

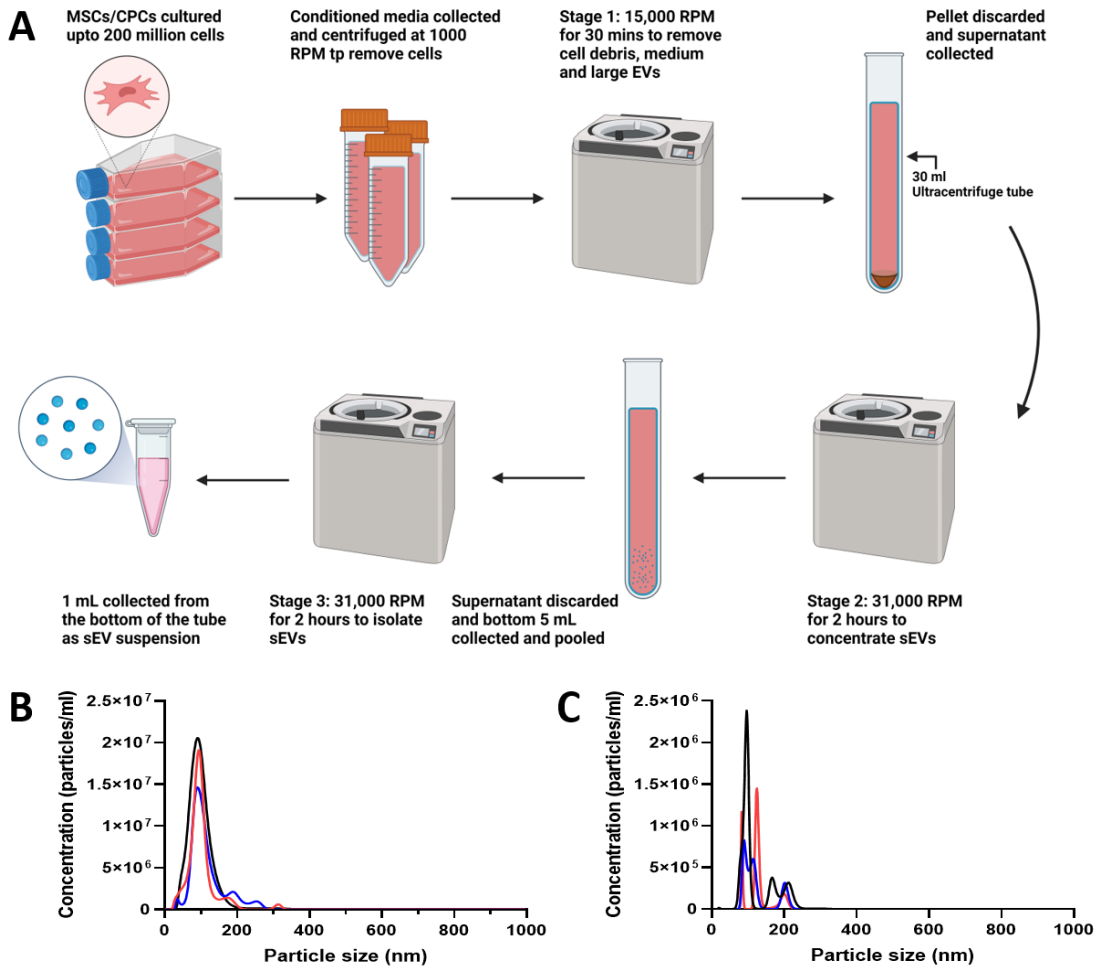

Figure 9- Isolation and characterization of CPC and MSC derived sEVs. (A) Optimized protocol for pure sEV isolation from cells. (B) NTA curves for CPC-sEVs (n=3) (C) NTA curves for MSC-sEVs (n=3)

4.4 Functional characterization of CPC sEVs

The administration of CPC sEVs has shown improvement in cardiac function by promoting angiogenesis in several animal models[71]. Recently, Sluijter et. al. have shown that the surface proteins, particularly, pregnancy associated plasma protein- A (PAPP-A) which is highly enriched in CPCs, are responsible for promoting sEV mediated

angiogenesis in endothelial cells via downstream signaling through the AKT and MAPK pathways[18]. Tube formation assay was used to assess the angiogenic ability of the isolated CPC sEVs. The addition of CPC sEVs induced the formation of tubes by HUVECs plated on Geltrex® coated wells. It is important to note that the HUVECs were quiesced before seeding to ensure that the increased tube formation was only a function of the sEVs. A significant increase in the number of branches, branch length and the overall tube length was observed in the treatment group when compared to the negative control proving that the CPC sEVs have a high angiogenic potential (**Figure 10**).

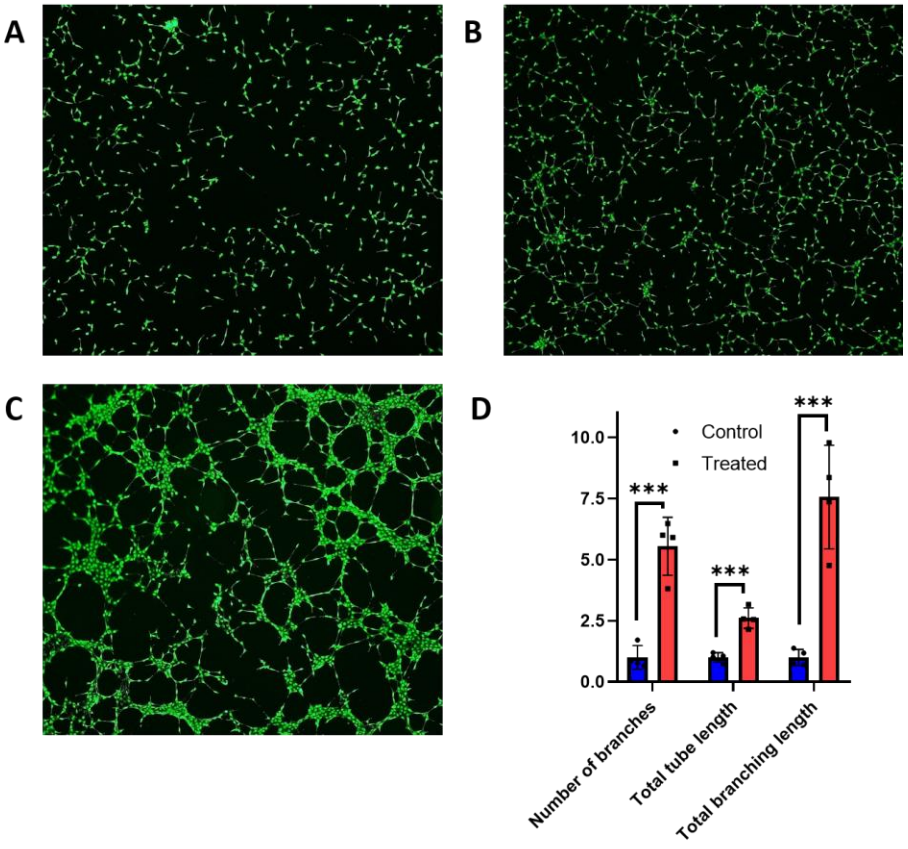

Figure 10- Tube formation assay for CPC-sEVs. Images were taken after 12 hours of incubation followed by staining with Calcein-AM for 30 mins. (A) Negative control cultured with EBM (B) Treatment group cultured with CPC-sEVs and EBM (C) Positive

control cultured with EGM (D) Comparison of tube parameters between control and treatment group. *** $p < 0.001$ (n=4)

Scratch wound healing assay was used to assess the pro-migratory potential of the CPC sEVs towards endothelial cells. It was observed that the average width and area of the scratch introduced in a HUVEC monolayer was significantly lower in the treated group compared to the negative control owing to the pro-migratory signals delivered by the CPV-sEVs (**Figure 11**).

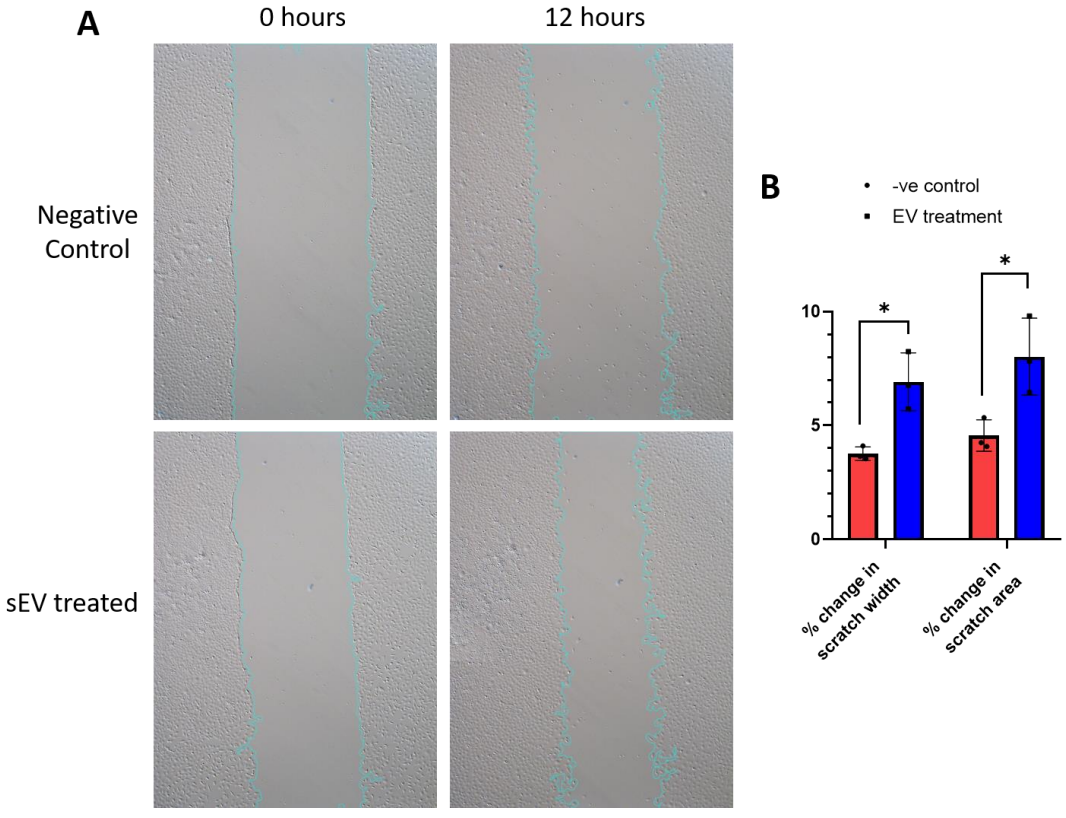

Figure 11- Scratch wound healing assay for CPC-sEVs. (A) Brightfield images of the scratch wound on HUVEC monolayers in the control and treatment group at 0 hours and 12 hours. The boundary of the wound is shown by the blue line (B) Comparison of the wound closure parameters between the control and the treatment group. * $p < 0.05$ (n=3)

4.5 sEV distribution and controlled release from GelMA-sEV patch

To visualize the distribution of sEVs in the patch and quantify their subsequent release, the sEVs were stained with a fluorescent dye. DiO has been used previously to stain sEVs[54] and was chosen for this study because of its highly lipophilic nature and strong affinity for lipid membranes. sEVs and the dye were mixed in the ratio 20 billion EVs to 20 µL of 1mM DiO and any excess dye was removed via dialysis for optimum staining. The ratio of DiO and sEVs was optimized well because a lower amount of dye will not stain all sEVs and a higher amount will precipitate out to form nanoclusters which cannot be distinguished from the sEVs. Further, the DiO staining renders the sEVs fluorescent in the 480 to 510 nm wavelength range which is the same as the PLGA NPs used previously. Thus, the same procedures can be used to assess their distribution and release. GelMA-sEV patches were printed using the bioink loaded with DiO stained sEVs and imaged using a confocal microscope. **Figure 12A** shows the maximum intensity projection of the Z stack images of the patch. Several images at 4x magnification were taken and stitched together to visualize the whole patch and the sEVs are observed to be uniformly distributed throughout the printed construct. **Figure 12B** shows a 3D reconstitution of the GelMA-sEV patch. The patch has diameter of approximately 10 mm with the thickness of 1 mm showing good fidelity with the CAD design and the sEVs are homogenously distributed across the thickness of the patch too. This proves that the sEVs do not aggregate inside the bioink. Next, the release of sEVs in PBS was assessed. Similar to the release profile of the GelMA-NP patches, the GelMA-sEV patches also had an initial burst release of approximately 35% of the payload during the first 6 hours followed by a sustained release of approximately 70% over 14 days (**Figure 12C**). The relatively slower release of the

sEVs compared to the NPs may be attributed to possible EV-matrix interactions. As shown ahead, such interactions do not hamper the functionality of the sEVs. Thus, the GelMA-sEV patch is effectively able to sustain the release of CPC-sEVs over a period of 2 weeks.

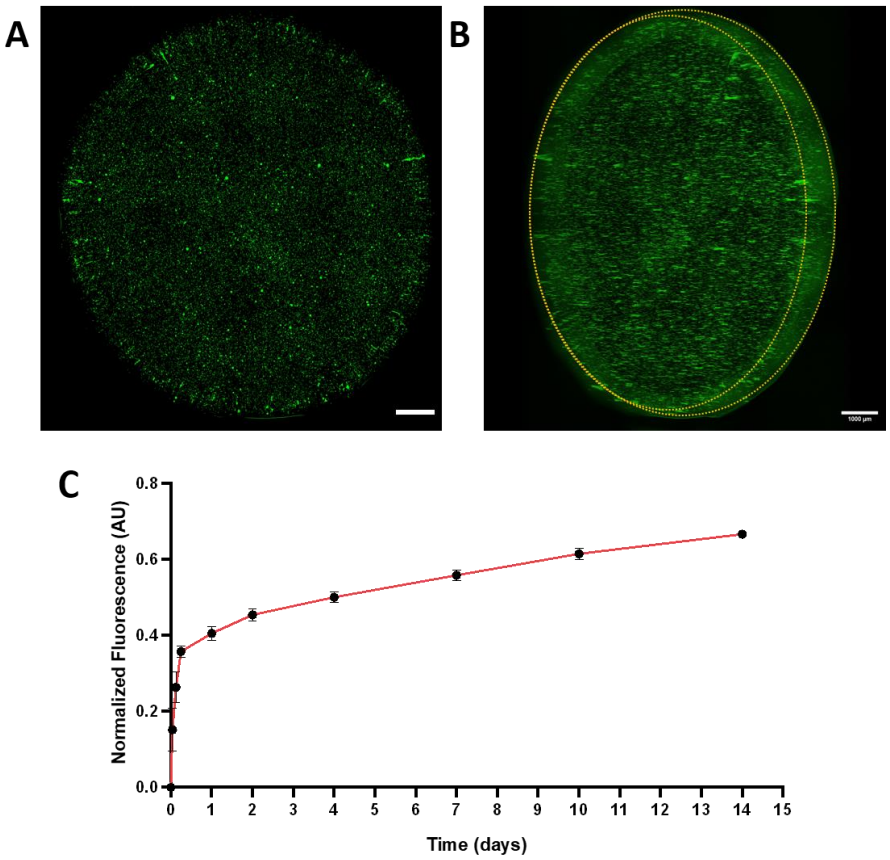

Figure 12- sEV distribution and release from GelMA-sEV patches. GelMA-sEV patch was printed with sEVs stained by DiO. (A) Maximum intensity projection of the z stack images for the patch (B) 3D projection of the GelMA-sEV patch turned at an angle of 30^0 around the Y-axis (C) Release profile of sEVs in PBS. (n=4)

4.6 Scratch wound healing assay with GelMA-sEV patch

Our next goal was to check whether the CPC-sEVs remained functional after their encapsulation and release from a GelMA scaffold. To do so we perform the scratch wound healing assay wherein the HUVECs were preconditioned with the GelMA-sEV patch for 2 days using a transwell insert to form a confluent monolayer before making the scratch (**Figure 13B**)**.** We hypothesized that during these 2 days, the patch would release approximately 50% of its encapsulated sEVs which can be taken up by the growing HUVECs and induce a pro-migratory phenotype in the cells. The control group is treated with a GelMA patch without encapsulated sEVs. We observed that the cells pretreated with the patch had a better migration of HUVECs as evidenced by a significantly higher wound closure compared to the negative controls (**Figure 13C**). This proves that CPC sEVs were released from the patch during the 2 days of incubation and were taken up the HUVECs and also that the pro-migratory functionality is not due to GelMA degradation products. Furthermore, the CPC-sEVs were able to retain their pro-migratory functionality even after encapsulation in a hydrogel matrix and were not negatively affected by interactions with GelMA. Thus, we believe that GelMA is a highly compatible material for holding sEVs as also suggested by Wu et. al.[72]. Further work is required to assess whether the sEVs are able to retain their shape and surface markers after encapsulation and release from the scaffold. This can be done by taking SEM/TEM images of the sEVs and performing western blot analysis on the sEVs before and after their release from the GelMA patch.

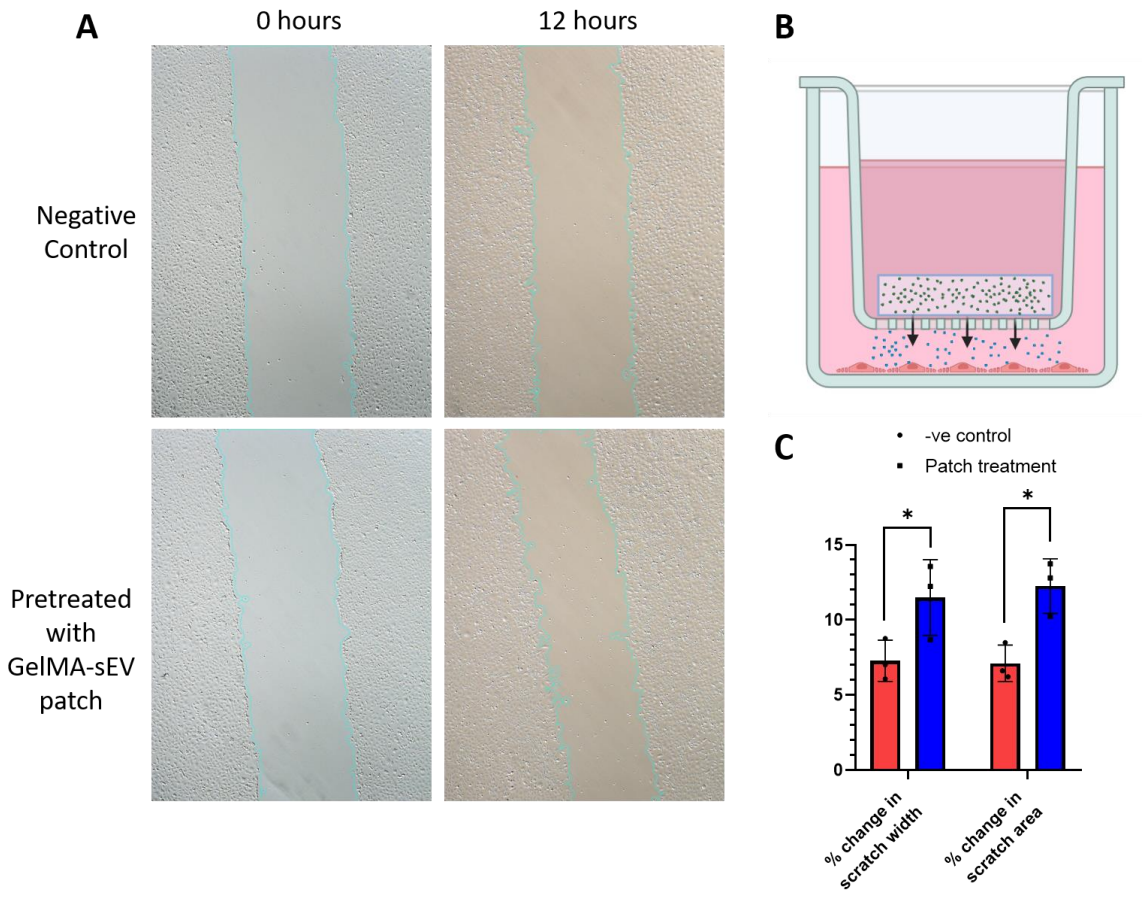

Figure 13- Scratch wound healing assay for GelMA-sEV patch. (A) Brightfield images of the scratch wound on HUVEC monolayers in the control and treatment group at 0 hours and 12 hours. The boundary of the wound is shown by the blue line (B) Experimental setup showing the GelMA-sEV patch on the transwell insert and HUVECs plated in the well and interacting with the CPC-sEVs (C) Comparison of the wound closure parameters between the control and the treatment group. * $p < 0.05$ (n=3)

4.7 HUVEC proliferation assay with GelMA-sEV patch

After showing that the sEVs released by the GelMA-sEV patch were able to promote HUVEC migration, we also wanted to check if the GelMA-sEV patch is able to promote their proliferation too. To do so, we used the MTS assay, a colorimetric metabolic assay

that quantifies the amount of live mammalian cells in a culture. We hypothesized that if the same number of HUVECs were seeded on a patch with and without encapsulated sEVs and allowed to culture for 1 or 2 days, the patch with sEVs (GelMA-sEV) will have a higher number of HUVECs and therefore an increased absorbance signal in the MTS assay due to increased proliferation. It is important to note that all cells were quiesced before seeding them on the patches and EBM was used to culture the HUVECs after seeding. This was done to ensure that the hypothesized increased proliferation due to sEVs was not overshadowed by proliferation due to the EGM. Before setting up the experiment, we optimized the number of cells to be seeded on the patches according to the sensitivity of the assay as too few cells will not give a proper colorimetric signal and too many will saturate it beyond the range of the assay, giving incorrect measurements. Besides, we also optimized the incubation time of the MTS reagent with the cells to prevent oversaturation of the signal as the extent of color change depends on the incubation time too. To do so, the MTS assay was performed on different concentrations of quiesced HUVECs with incubation times of 1, 2 or 3 hours (**Figure 14**). 1 hour was chosen as the optimum incubation time as it allowed for the longest detection range of cell concentrations. Both 2 hours and 3 hours of incubation caused saturation at the concentration of 8×10^4 cells. Further, the concentration of 2×10^4 cells was chosen as the seeding density for the proposed experiment as the increase in absorbance from 2×10^4 cells followed a linear trend which will be able to quantify the cell proliferation most accurately.

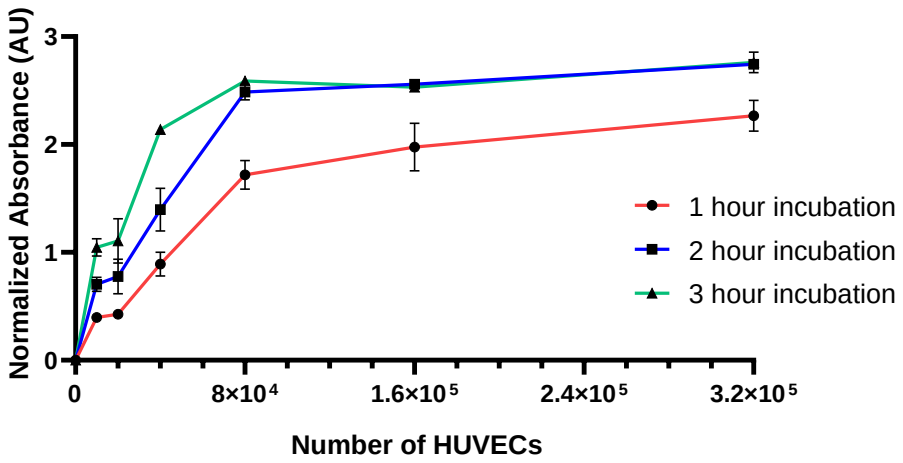

Figure 14- Optimizing HUVEC loading and incubation time for MTS assay

The experiment was designed with 6 groups as shown in **Figure 15A** and two experimental sets with six groups in each were used. Briefly, HUVECs were quiesced overnight, prior to the start of the experiment. On day 0, cells were seeded in both the experimental sets as previously described. After 16 hours, the MTS assay was performed on experimental set 1 and the day 1 absorbance readings were obtained using a plate reader. After 40 hours, the assay was performed on experimental set 2 and the day 2 absorbance readings were measured. It was observed in the group 2 that the GelMA patch (without any cells) was also responsive to the MTS assay leading to a color change. The absorbance of group 2 was thus used as the baseline and was subtracted from the group 4 and group 5 absorbances before analysis. We found that the group with GelMA-sEV patches had a greater number of HUVECs compared to the GelMA only patch group on both day 1 and day 2 evidenced by its higher absorbance in the MTS assay (**Figure 15B**). This can be attributed to the pro-proliferative effects of the CPC-sEVs released from the patch.

After the MTS assay on day 1 and day 2, the patches were removed from the groups 4,5 and 6, the cells in the well were washed twice with PBS and stained with Calcein-AM for visualization (**Figure 15C**). When the HUVECs are seeded on the patches on day 0, while some cells adhere to the patch, many of them slide down and attach to the bottom of the well around the patch as the patch diameter is slightly less than the well diameter. We wanted to wanted to make visual inferences about the number and condition of these cells in groups 4,5 and 6 on day 1 and day 2. We observed that the Group 6 which received EGM had the highest number of cells for both day 1 and day 2 and the cells appeared to be the healthiest among the 3 groups, maintaining their morphology. The treatment group 5 had a greater number of HUVECs compared to the group 4 which received the blank GelMA patch and although the HUVEC size had shrunk for both the groups, the cells in group 5 appear bigger and healthier than those in group 4 for both day 1 and day 2. Using the MTS assay, we also observe that for the group 3 (cell control) the absorbance on day 2 was lower than that on day 1 (**Figure 15D**). This is because extended culture of HUVECs in EBM (serum free media) is bound to decrease their viability. This is also observed in the fluorescent images of the cells where the cells are more in number and healthier on day 1 as compared to day 2 and explains the decrease in absorbance on day 2 compared to day 1 in the **Figure 15B.** The observation that the number of HUVECs is more in the GelMA-sEV treated group than in the GelMA treated group even on day 2 suggests that even if there is no further cell proliferation between day 1 and day 2, the sEV loaded patch was able to reduce death of the strained HUVECs in nutrient deficit conditions.

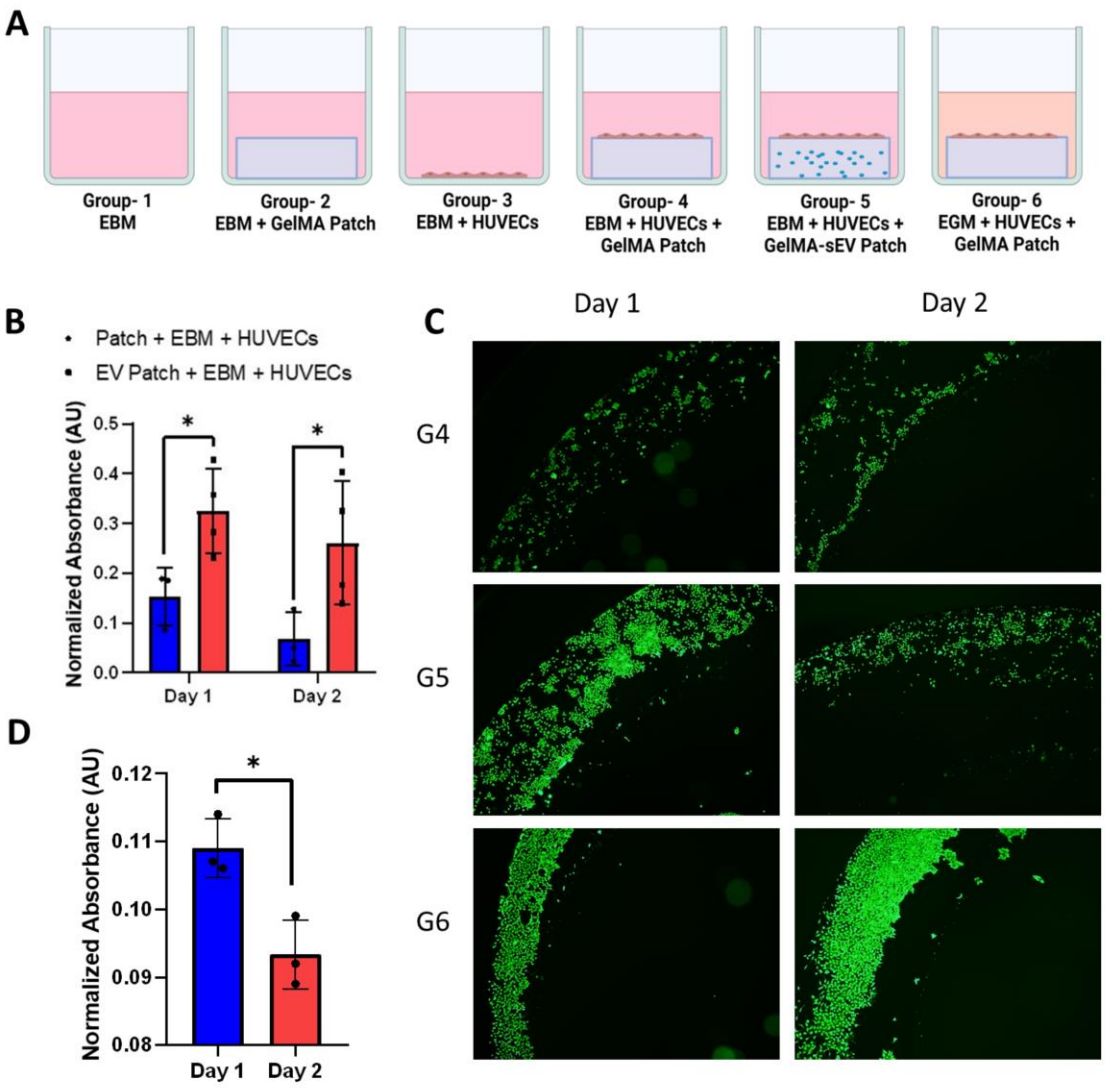

Figure 15- MTS cell proliferation assay for GelMA-sEV patch. (A) 6 groups used for testing the pro-proliferative potential of the GelMA-sEV patch (B) Comparison of the MTS assay absorbance for the HUVECs in Group 4 and Group 5 (C) Calcein-AM stained HUVECs in Groups 4, 5 and 6 for day 1 and day 2 (D) Comparison of the MTS assay absorbance for the HUVECs in Group 3 for day 1 and day 2. * $p < 0.05$ (n=3)

CHAPTER 5. CONCLUSIONS AND FUTURE DIRECTIONS

In this study, we developed a completely cell-free cardiac patch loaded with CPC derived small extracellular vesicles using 3D extrusion bioprinting. We first isolated sEVs from neonatal patient derived CPCs and showed that they had a strong angiogenic and pro-migratory potential. By encapsulating the sEVs in a bioprinted GelMA patch, we were able to sustain their release for over 14 days which is perfect for targeting the cardiac tissue remodeling phase post MI. We showed that the sEVs released from the patch retained their functionality and that the GelMA-sEV patch was able to significantly improve migration and proliferation of HUVECs in-vitro. While the results are promising, further experimentation is required before transitioning to in-vivo studies. Firstly, the stiffness of the patch must be measured and optimized to mimic the stiffness of cardiac tissue. Secondly, a more appropriate method for measuring sEV release from the patch must be used which takes into account the enzymatic degradation of the patch due to physiological proteases along with the stretching and shearing forces that would be experienced by a patch implanted on the heart. Further, the pore size of the GelMA scaffold in the patch must be measured, compared with the sEV size to make sure that the pre and post swelling pore size is less than and more than the sEV diameter respectively. Finally, this study only addresses the effect of sEVs and the GelMA-sEV patch on endothelial cells and their effect on cardiomyocytes has not been explored. We believe that based on previously published literature, the CPC sEVs and the patch encapsulating them will have a pro-proliferative and pro-migratory effect on the CMCs and exploring this aspect will further strengthen our study.

3D bioprinting provides a highly modular way to fabricate sEV loaded cardiac patches. While this study explores a GelMA based bioink for encapsulating CPC derived sEVs, this approach can also be extended to encapsulate sEVs from other sources by simply pre-mixing in the bioink. Besides, other signaling molecules such as growth factors can be easily added to the patch for augmenting its functionality. Further, higher or lower concentrations of GelMA can be used to tune the sEV release profile and other biomaterials such alginate or decellularized cardiac ECM can be added to the bioink to enhance the regenerative potential of the scaffold. To fully utilize the flexibility provided by the bioprinter, complex patches with predesigned vasculature can be printed to allow better interaction of the scaffold with the cardiac tissue.

To conclude, this proof of concept study effectively highlights the potential of 3D bio-printed sEVs in cardiac regeneration, a previously unexplored niche. We successfully developed a functional platform that than retain sEVs at the site of cardiac tissue injury, overcoming the issue of fast their fast clearance. The platform has the potential to be improved and tested further to obtain more robust results and the cell-free approach makes it more easily translatable into clinical settings.

REFERENCES

1. Salari, N. *et al.* The global prevalence of myocardial infarction: a systematic review and meta-analysis. *BMC Cardiovasc. Disord.* **23**, 1–12 (2023).

2. Saleh, M. & Ambrose, J. A. Understanding myocardial infarction [version 1; referees: 2 approved]. *F1000Research* **7**, 1–8 (2018).

3. Foglia, M. J. & Poss, K. D. Building and re-building the heart by cardiomyocyte proliferation. *Dev.* **143**, 729–740 (2016).

4. Wu, C., Liu, B., Wang, R. & Li, G. The Regulation Mechanisms and Clinical Application of MicroRNAs in Myocardial Infarction: A Review of the Recent 5 Years. *Front. Cardiovasc. Med.* **8**, 1–15 (2021).

5. Han, C. *et al.* Human umbilical cord mesenchymal stem cell derived exosomes encapsulated in functional peptide hydrogels promote cardiac repair. *Biomater. Sci.* **7**, 2920–2933 (2019).

6. Bheri, S., Kassouf, B. P., Park, H. J., Hoffman, J. R. & Davis, M. E. Engineering cardiac small extracellular vesicle-derived vehicles with thin-film hydration for customized microRNA loading. *J. Cardiovasc. Dev. Dis.* **8**, (2021).

7. Hsieh, P. C. H. *et al.* Evidence from a genetic fate-mapping study that stem cells refresh adult mammalian cardiomyocytes after injury. *Nat. Med.* **13**, 970–974 (2007).

8. Yu, T. *et al.* In vivo differentiation of induced pluripotent stem cell-derived cardiomyocytes. *Circ. J.* **77**, 1297–1306 (2013).

9. Mingliang, R., Bo, Z. & Zhengguo, W. Stem cells for cardiac repair: Status, mechanisms, and new strategies. *Stem Cells Int.* **2011**, (2011).

10. Wang, Z. Assessing Tumorigenicity in Stem Cell-Derived Therapeutic Products: A Critical Step in Safeguarding Regenerative Medicine. *Bioengineering* **10**, (2023).

11. Lemcke, H., Voronina, N., Steinhoff, G. & David, R. Recent Progress in Stem Cell Modification for Cardiac Regeneration. *Stem Cells Int.* **2018**, (2018).

12. Fang, Y. H. *et al.* Immunogenicity in stem cell therapy for cardiac regeneration. *Acta Cardiol. Sin.* **36**, 588–594 (2020).

13. Povsic, T. J. Approaching regulatory approval of cardiovascular regenerative therapy. *Circ. Res.* **122**, 552–554 (2018).

14. Hodgkinson, C. P., Bareja, A., Gomez, J. A. & Dzau, V. J. Emerging Concepts in Paracrine Mechanisms in Regenerative Cardiovascular Medicine and Biology. *Circ. Res.* **118**, 95–107 (2016).

15. Liu, L. *et al.* Exosomes Derived from Mesenchymal Stem Cells Rescue Myocardial Ischaemia/Reperfusion Injury by Inducing Cardiomyocyte Autophagy Via AMPK and Akt Pathways. *Cell. Physiol. Biochem.* **43**, 52–68 (2017).

16. S., D. *et al. Cardioprotective Effects of Exosomes and Their Potential Therapeutic Use. Advances in experimental medicine and biology* vol. 998 (2017).

17. Yang, P. C. Induced pluripotent stem cell (iPSC)-derived exosomes for precision medicine in heart failure. *Circ. Res.* **122**, 661–663 (2018).

18. Roefs, M. T. *et al.* Cardiac progenitor cell-derived extracellular vesicles promote angiogenesis through both associated- and co-isolated proteins. *Commun. Biol.* **6**, 1–16 (2023).

19. Wang, X. *et al.* Engineered exosomes with ischemic myocardium-targeting peptide for targeted therapy in myocardial infarction. *J. Am. Heart Assoc.* **7**, 1–16 (2018).

20. Geng, T. *et al.* Recent Advancement and Technical Challenges in Developing Small Extracellular Vesicles for Cancer Drug Delivery. *Pharm. Res.* **38**, 179–197 (2021).

21. Zhou, X., Jia, Y., Mao, C. & Liu, S. Small extracellular vesicles: Non-negligible vesicles in tumor progression, diagnosis, and therapy. *Cancer Lett.* **580**, 216481 (2024).

22. Lu, Y., Wang, L., Zhang, M. & Chen, Z. Mesenchymal Stem Cell-Derived Small Extracellular Vesicles: A Novel Approach for Kidney Disease Treatment. *Int. J. Nanomedicine* **17**, 3603–3618 (2022).

23. Ju, Y., Hu, Y., Yang, P., Xie, X. & Fang, B. Extracellular vesicle-loaded hydrogels for tissue repair and regeneration. *Mater. Today Bio* **18**, 100522 (2023).

24. Barile, L. *et al.* Extracellular vesicles fromhuman cardiac progenitor cells inhibit cardiomyocyte apoptosis and improve cardiac function aftermyocardial infarction. *Cardiovasc. Res.* **103**, 530–541 (2014).

25. Morishita, M. *et al.* Quantitative analysis of tissue distribution of the B16BL6-derived exosomes using a streptavidin-lactadherin fusion protein and Iodine-125-Labeled biotin derivative after intravenous injection in mice. *J. Pharm. Sci.* **104**, 705–713 (2015).

26. Gallet, R. *et al.* Exosomes secreted by cardiosphere-derived cells reduce scarring, attenuate adverse remodelling, and improve function in acute and chronic porcine myocardial infarction. *Eur. Heart J.* **38**, 201–211 (2017).

27. Huang, M. *et al.* Hydrogels for the treatment of oral and maxillofacial diseases: current research, challenges, and future directions. *Biomater. Sci.* **10**, 6413–6446 (2022).

28. Buwalda, S. J. *et al.* Hydrogels in a historical perspective: From simple networks to smart materials. *J. Control. Release* **190**, 254–273 (2014).

29. Hashemi, A., Ezati, M., Nasr, M. P., Zumberg, I. & Provaznik, V. Extracellular Vesicles and Hydrogels: An Innovative Approach to Tissue Regeneration. *ACS Omega* **9**, 6184–6218 (2024).

30. Pu, Y. *et al.* Extracellular Vesicles from NMN Preconditioned Mesenchymal Stem Cells Ameliorated Myocardial Infarction via miR-210-3p Promoted Angiogenesis. *Stem Cell Rev. Reports* **19**, 1051–1066 (2023).

31. Zhu, D. *et al.* Minimally invasive delivery of therapeutic agents by hydrogel injection into the pericardial cavity for cardiac repair. *Nat. Commun.* **12**, 1–10 (2021).

32. Lv, K. *et al.* Incorporation of small extracellular vesicles in sodium alginate hydrogel as a novel therapeutic strategy for myocardial infarction. *Theranostics* **9**, 7403–7416 (2019).

33. Han, P. & Ivanovski, S. 3D bioprinted extracellular vesicles for tissue engineering—a perspective. *Biofabrication* **15**, (2023).

34. Jiao, K. *et al.* Bioprinting extracellular vesicles as a 'cell-free' regenerative medicine approach. *Extracell. Vesicles Circ. Nucleic Acids* **4**, 218–239 (2023).

35. Ning, L. *et al.* Biomechanical factors in three-dimensional tissue bioprinting. *Appl. Phys. Rev.* **7**, (2020).

36. Wang, Z. *et al.* 3D bioprinting in cardiac tissue engineering. *Theranostics* **11**, 7948–7969 (2021).

37. Yerneni, S. S., Whiteside, T. L., Weiss, L. E. & Campbell, P. G. Bioprinting exosome-like extracellular vesicle microenvironments. *Bioprinting* **13**, e00041 (2019).

38. Sun, X. *et al.* Mesenchymal Stem Cell-Derived Exosomes Enhance 3D-Printed Scaffold Functions and Promote Alveolar Bone Defect Repair by Enhancing Angiogenesis. *J. Pers. Med.* **13**, (2023).

39. Zha, Y. *et al.* Progenitor cell-derived exosomes endowed with VEGF plasmids enhance osteogenic induction and vascular remodeling in large segmental bone defects. *Theranostics* **11**, 397–409 (2020).

40. Yang, T. *et al.* Sustained Release of BMSC-EVs from 3D Printing Gel/HA/nHAP Scaffolds for Promoting Bone Regeneration in Diabetic Rats. *Adv. Healthc. Mater.* **12**, (2023).

41. Ma, S. *et al.* Functionalized 3D Hydroxyapatite Scaffold by Fusion Peptides-Mediated Small Extracellular Vesicles of Stem Cells for Bone Tissue Regeneration. *ACS Appl. Mater. Interfaces* **16**, 3064–3081 (2024).

42. Chen, P. *et al.* Desktop-stereolithography 3D printing of a radially oriented extracellular matrix/mesenchymal stem cell exosome bioink for osteochondral defect regeneration. *Theranostics* **9**, 2439–2459 (2019).

43. Sun, T. *et al.* Novel 3D-printing bilayer GelMA-based hydrogel containing BP, β-TCP and exosomes for cartilage-bone integrated repair. *Biofabrication* **16**, (2024).

44. Li, X.-R. *et al.* Three-dimensional printed biomimetic multilayer scaffolds coordinated with sleep-related small extracellular vesicles: A strategy for extracellular matrix homeostasis and macrophage polarization to enhance osteochondral regeneration. *VIEW* (2024) doi:10.1002/VIW.20230069.

45. Ding, Z. *et al.* Apoptotic extracellular vesicles derived from hypoxia-preconditioned mesenchymal stem cells within a modified gelatine hydrogel promote osteochondral regeneration by enhancing stem cell activity and regulating immunity. *J. Nanobiotechnology* **22**, (2024).

46. Liu, X.-Y. *et al.* Low-temperature 3D-printed collagen/chitosan scaffolds loaded with exosomes derived from neural stem cells pretreated with insulin growth factor-

1 enhance neural regeneration after traumatic brain injury. *Neural Regen. Res.* **18**, 1990–1998 (2023).

47. Liu, X. *et al.* Integrated printed BDNF-stimulated HUCMSCs-derived exosomes/collagen/chitosan biological scaffolds with 3D printing technology promoted the remodelling of neural networks after traumatic brain injury. *Regen. Biomater.* **10**, (2023).

48. Ferroni, L. *et al.* Stem cell-derived small extracellular vesicles embedded into methacrylated hyaluronic acid wound dressings accelerate wound repair in a pressure model of diabetic ulcer. *J. Nanobiotechnology* **21**, (2023).

49. Bar, A., Kryukov, O. & Cohen, S. Three-Dimensional Bio-Printed Cardiac Patch for Sustained Delivery of Extracellular Vesicles from the Interface. *Gels* **8**, (2022).

50. Bar, A., Kryukov, O., Etzion, S. & Cohen, S. Engineered extracellular vesicle-mediated delivery of miR-199a-3p increases the viability of 3D-printed cardiac patches. *Int. J. Bioprinting* **9**, 316–330 (2022).

51. Maiullari, F. *et al.* In vivo organized neovascularization induced by 3D bioprinted endothelial-derived extracellular vesicles. *Biofabrication* **13**, (2021).

52. Born, L. J. *et al.* Sustained released of bioactive mesenchymal stromal cell-derived extracellular vesicles from 3D-printed gelatin methacrylate hydrogels. *J. Biomed. Mater. Res. - Part A* **110**, 1190–1198 (2022).

53. Bari, E. *et al.* Silk Fibroin Bioink for 3D Printing in Tissue Regeneration: Controlled

Release of MSC extracellular Vesicles. *Pharmaceutics* **15**, (2023).

54. Han, P. *et al.* 3D bioprinted small extracellular vesicles from periodontal cells enhance mesenchymal stromal cell function. *Biomater. Adv.* **158**, (2024).

55. Maiullari, F. *et al.* A multi-cellular 3D bioprinting approach for vascularized heart tissue engineering based on HUVECs and iPSC-derived cardiomyocytes. 1–15 (2018) doi:10.1038/s41598-018-31848-x.

56. Gao, L. *et al.* Myocardial Tissue Engineering with Cells Derived from Human-Induced Pluripotent Stem Cells and a Native-Like, High-Resolution, 3-Dimensionally Printed Scaffold. *Circ. Res.* **120**, 1318–1325 (2017).

57. Pepelanova, I., Kruppa, K., Scheper, T. & Lavrentieva, A. Gelatin-methacryloyl (GelMA) hydrogels with defined degree of functionalization as a versatile toolkit for 3D cell culture and extrusion bioprinting. *Bioengineering* **5**, (2018).

58. Bejleri, D. *et al.* A Bioprinted Cardiac Patch Composed of Cardiac-Specific Extracellular Matrix and Progenitor Cells for Heart Repair. *Adv. Healthc. Mater.* **7**, 1–13 (2018).

59. Ouyang, L., Yao, R., Zhao, Y. & Sun, W. Effect of bioink properties on printability and cell viability for 3D bioplotting of embryonic stem cells. *Biofabrication* **8**, (2016).

60. Hosseini, V. *et al.* Engineered contractile skeletal muscle tissue on a microgrooved methacrylated gelatin substrate. *Tissue Eng. - Part A* **18**, 2453–2465 (2012).

61. Billiet, T., Gevaert, E., De Schryver, T., Cornelissen, M. & Dubruel, P. The 3D printing of gelatin methacrylamide cell-laden tissue-engineered constructs with high cell viability. *Biomaterials* **35**, 49–62 (2014).

62. Gao, G. *et al.* Improved properties of bone and cartilage tissue from 3D inkjet-bioprinted human mesenchymal stem cells by simultaneous deposition and photocrosslinking in PEG-GelMA. *Biotechnol. Lett.* **37**, 2349–2355 (2015).

63. Shin, S. R. *et al.* Reduced graphene oxide-GelMA hybrid hydrogels as scaffolds for cardiac tissue engineering. *Small* **12**, 3677–3689 (2016).

64. Tang, L. *et al.* GelMA Hydrogel Loaded with Extracellular Vesicles Derived from Umbilical Cord Mesenchymal Stem Cells for Promoting Cutaneous Diabetic Wound Healing. *ACS Omega* **8**, 10030–10039 (2023).

65. Tang, J. *et al.* Injection-Free Delivery of MSC-Derived Extracellular Vesicles for Myocardial Infarction Therapeutics. *Adv. Healthc. Mater.* **11**, 1–14 (2022).

66. Nguyen, A. K., Goering, P. L., Reipa, V. & Narayan, R. J. Toxicity and photosensitizing assessment of gelatin methacryloyl-based hydrogels photoinitiated with lithium phenyl-2,4,6-trimethylbenzoylphosphinate in human primary renal proximal tubule epithelial cells. *Biointerphases* **14**, (2019).

67. Shah, A. M. & Mann, D. L. In search of new therapeutic targets and strategies for heart failure: Recent advances in basic science. *Lancet* **378**, 704–712 (2011).

68. van der Laan, A. M., Piek, J. J. & van Royen, N. Targeting angiogenesis to restore

the microcirculation after reperfused MI. *Nat. Rev. Cardiol.* **6**, 515–523 (2009).

69. Scalise, R. F. M. *et al.* Fibrosis after Myocardial Infarction: An Overview on Cellular Processes, Molecular Pathways, Clinical Evaluation and Prognostic Value. *Med. Sci. (Basel, Switzerland)* **9**, (2021).

70. Almeria, C., Kreß, S., Weber, V., Egger, D. & Kasper, C. Heterogeneity of mesenchymal stem cell-derived extracellular vesicles is highly impacted by the tissue/cell source and culture conditions. *Cell Biosci.* **12**, 1–15 (2022).

71. Yang, L. *et al.* Aging-11-101814. **11**, (2019).

72. Wu, K. *et al.* Preservation of small extracellular vesicle in gelatin methacryloyl hydrogel through reduced particles aggregation for therapeutic applications. *Int. J. Nanomedicine* **16**, 7831–7846 (2021).